Hindawi
International Journal of Photoenergy
Volume 2022, Article ID 3869867, 22 pages
https://doi.org/10.1155/2022/3869867

Research Article

Completely Recuperative Supercritical CO_2 Recompression Brayton/Absorption Combined Power/Cooling Cycle: Performance Assessment and Optimization

Bing-Chuan Han,[1] **Yong-Dong Chen**,[1,2] **Gai-Ge Yu**,[1] **Xiao-Hong Wu**,[1] **and Tao-Tao Zhou**[3]

[1]*Hefei General Machinery Research Institute, Hefei, Anhui 230031, China*
[2]*State Key Laboratory of Compressor Technology, Hefei General Machinery Research Institute, Hefei 230031, China*
[3]*School of Automotive and Transportation Engineering, Hefei University of Technology, Hefei, Anhui 230031, China*

Correspondence should be addressed to Yong-Dong Chen; chenyongdong@hgmri.com

Received 8 March 2022; Revised 12 April 2022; Accepted 20 April 2022; Published 20 May 2022

Academic Editor: Qiliang Wang

Excessive heat losses and water consumption in cooling units are significant constraints restricting the application circumstances and performances for the SCO_2 Brayton cycle, and the heat exchange capacity in the precooler (PRC) is typically 1.5 times that of power generation. Therefore, this research offers a high-integrated combined power/cooling system in which two waste heat exchangers (WHEs) and a rectifier (RET) are used instead of the PRC to achieve 100% exhaust heat recovery. Each component's energy and exergy models are developed, and the operational characteristics, coupling relationships, and exergy destruction distribution are examined. Results indicate that, when compared to the Brayton cycle, the thermal and exergy efficiency is considerably increased, and the concentration difference and WHE1 pitch point difference have significant influences on system performance. Further exergoeconomic and optimization analysis reveals that the superior exergy case is mostly recommended for relevant thermal and exergy efficiency increasing rates of 13.7% and 9.17%, respectively, and the unit cost is 81.33% that of the base case. Turbine 1 (TUR1) and main compressor (MCP) are the first and second highest cost rates, respectively, and RET and generator (GEN) account for roughly 34% exergy destruction rate and 20% exergy destruction cost rate, respectively. In addition, reducing heat transfer differences in relevant equipment can further promote system performance.

1. Introduction

Global environmental pollution issues concerning ozone depletion, excess emission of carbon dioxide, and growing demand for energy consumption have aroused widespread focus on the efficient utilization of primary energy and the development of sustainable energy use technologies [1, 2]. Efficient and low-carbon or even zero-carbon energy conversion systems that can meet different renewable energy requirements for multiple heat source applications have become an important research subject [3, 4]. In recent years, Supercritical Carbon Dioxide (SCO_2) has attracted the attention of many scholars as an efficient and pollution-free clean cycle working fluid, and research on the SCO_2 Brayton cycle has gradually become a hotspot [5, 6]. For instance, concentrated solar power (CSP) and nuclear power integrated SCO_2 Brayton cycle for distributed power systems have been promising application prospects in the increasingly severe global circumstances of implementation in carbon neutrality and carbon peaking [7, 8].

For major clean energy power generation applications such as geothermal power plants, natural gas stations, concentrated solar power plants, fuel cells, generation IV nuclear power plants, and fusion reactors, the SCO_2 Brayton cycle is considered to be the most promising alternative power system due to its layout simplicity, investment economy, size compactness, and intrinsic safety [9–12]. The SCO_2 Brayton cycle, first proposed by Feher and Angelino

in 1967, was operated at temperatures and pressures above the critical point (31.1°C and 7.39 MPa, respectively) for the entire cycle [13, 14]. The temperature and pressure at the inlet point of the compressor were slightly higher than the critical point, and the density of carbon dioxide was close to that of liquid and difficult to be compressed; therefore, the size and power consumption can be significantly reduced. In recent years, many researchers and institutions built various engineering prototypes and verified the feasibility of the system [3, 5].

A simple Brayton cycle, recompression cycle, intercooling cycle, and reheating cycle are typical operation conditions aimed at efficiency increase in power generation, and in these cycles, the exhausting heat in the precoolers is ultimately discharged to the environment; although it is low-grade heat at a temperature of about 150°C, the heat transfer capacity in the precoolers is generally 1.5 times that of the power generation capacity [15].

Although the Brayton cycles have many advantages in terms of performance and compactness, the high cost of heat exchangers (about 40% of the total investment cost) and large low-grade heat loss in the precooler (exceeding 55% of overall heat capacity provided) restricted their further development, promotion, and application [15–17]. The used heat exchangers which are called printed circuit heat exchangers (PCHE) have characteristics of high temperature, pressure resistance, and compact structure and are extremely expensive for the required typical manufacturing process involving chemical etching and diffusion bonding [18, 19]. In addition, when integrated with different solar concentration technologies such as solar power tower solar dish, parabolic trough collector, and linear Fresnel collector for regions with rich solar resources, the large amount of exhaust low-grade waste heat in low-temperature recuperator (LTR) ranging from 100 to 180°C is frequently cooled by open cooling water circulation in PRC, which not only caused the system efficiency for solar energy utilization to decrease but also limited its commercial engineering applications in arid inland regions for a lot of valuable water resources are consumed [20].

To improve the performance of the Brayton cycle, various combined systems with functional outputs are introduced to realize a further utilization of rejected heat; therefore, low boiling working medium power systems are employed as the bottom cycle [21]. Among them are two typical power cycles: the organic-temperature Rankine cycle and ammonia-water cycle [22]. The organic Rankine cycle which employed isobutane, isopentane, R114, etc. has the drawbacks of high cost and environmental pollution. The ammonia-water cycle, on the other hand, exhibited a variable temperature boiling process, which allowed maintenance of a fixed temperature difference with limited heat sources and less exergy loss. However, the variable temperature condensation process resulted in a low turbine expansion ratio and inefficiency. Kalina [23] introduced a power cycle which substituted the condensation process with an absorption process, attracting wide attention.

Since cooling/heating demand accounted for 40-50% of domestic power consumption, for the low-grade exhaust heat in the Brayton cycle, heat-driven absorption refrigeration also can be a promising alternative [24, 25]. Moreover, the operational temperature, pressure, and concentration have been complementary with ammonia-water power cycles; therefore, combined power/cooling systems have been widely concerned [26].

However, simply analyzing the thermal efficiency of the system can easily result in higher system unit costs [27, 28]. To accurately describe the impact of energy quality and unit cost on system performance, a thermoeconomic analysis methodology that takes into account the required capital investment, exergy inefficiencies, and the cost rates associated with these inefficiencies should be introduced as the main evaluation criterion in evaluating and optimizing thermal systems [29].

Optimization of thermal systems merely from the perspective of thermodynamics would always result in a high cost for the total system [30]. To accurately evaluate and promote the system performance, thermoeconomic analysis in a synthesis of exergy and economics perspectives should be advocated to perform a high-efficient and low-cost design and operation. To ameliorate this deficiency, several typical methodologies from the thermoeconomic point of view were developed and applied in recent years, thermoeconomic functional analysis (TFA), specific exergy costing approach (SPECO), and theory of the exergetic cost (TEC), for instance, and all proposed methodologies can be employed in the analysis of thermal systems principally.

The above efforts highlight the performance promotion potential of the Brayton combined systems, and it seems that the Brayton cycle integrating with low-grade heat utilization cycles is the most promising alternative for different heat source utilization occasions. Despite the large amounts of research in the case of the Brayton combined systems and to the best of the authors' knowledge, no attempt has been paid to achieve complete utilization of rejected heat in the precoolers. Furthermore, the complex coupling relations between different subcycles and components were hardly elaborated.

The present work is an effort to tackle these challenges. For this purpose, a novel system that has the characteristics of high integration and completely recuperative Brayton cycle in combination with an absorption cycle capable of power/cooling supply is proposed and analyzed. To accurately evaluate and promote the system performance, thermoeconomic analysis in a synthesis of exergy and economics perspectives is conducted to perform a high-efficient and low-cost design and operation. In addition, a parametric sensitivity analysis concerning a set of decision variables such as maximum temperature, maximum pressure, concentration, and the temperature difference is performed to identify the influence on thermal efficiency, exergy efficiency, and unit cost of products. Moreover, in various factors affecting the system performance, for which different variation trends are indicated, multiple key factors which influence the entire system performance should be evaluated simultaneously. For multiparameter optimization purposes, various optimization procedures are available; among them are the direct search method, Monte Carlo

method, and Genetic Algorithm (GA) method [31]. Considering the strong nonlinear constraints of the proposed system, the direct search method is applied in this paper from the view of the thermoeconomic approach. It is hoped that the results can provide some help in the development of attractive and efficient energy utilization systems.

2. System Description and Assumptions

A schematic diagram of the considered power/cooling integrated system is shown in Figure 1. And the cycle functions as a combination of power and cooling outputs as the main and side products, respectively.

As depicted in the proposed layout, for the SCO_2 Brayton subcycle represented by a solid yellow line, SCO_2 stream 1 which is slightly above the critical point entered the MCP and is compressed into a high pressure state of about 25 MPa; then, the stream leaving the MCP flowed to the LTR and recovered heat; then, the exiting stream 3a joins stream 3b at the recompression compressor (RCP) outlet and merges into a whole stream 3; afterwards, stream 3 is heated in the high-temperature recuperator (HTR) before entering the intermediate heat exchanger (IHE), and then, the stream absorbs heat from the high-temperature source (HTS) through IHE; the outlet stream flows to the TUR1, fully expands, and produces electricity in the power generation unit 1 (PGU1). The expanded stream 6 enters the HTR and LTR to heat stream 3 and stream 2, respectively. Stream 8 exiting the LTR is split into two streams: stream 8a and stream 8b. Stream 8a enters the waste heat recovery exchanger 1 (WHE1), the GEN, and the waste heat recovery exchanger 2 (WHE2) to heat the ammonia-water solution streams, respectively. And stream 8b flows into the RCP and further joins stream 3a exiting the LTR. For the absorption power/cooling subcycle represented by a solid blue line, the saturated high-concentration ammonia-water solution (referred to as rich solution) stream 31 leaving the absorber 2 (ABS2) is pressurized in the booster pump 2 (P2); then, the rich solution enters the WHE2 and the WHE1 to recovery heat from the SCO_2 stream, respectively, and became overheating vapor and then enters the turbine 2 (TUR2), expands under the condition of the minimum allowable dryness, and produces electricity in the power generation unit 2 (PGU2); after that, the exhaust steam in the TUR2 rejects heat in the solution heat recuperator 1 (SHR1) and mixes with low-concentration ammonia-water solution (referred to as poor solution) stream 30 in the absorber 1 (ABS1); then, the saturated medium concentration ammonia-water solution (referred to as basic solution) is pumped to a higher pressure in the booster pump 1 (P1) before splitting into two streams in the splitter (SPL): stream 16 and stream 17, and then, stream 16 enters the SHR1, solution heat recuperator 2 (SHR2), and RET to recovery heat, respectively; after that, the stream receives heat in the GEN and is separated into poor solution stream and ammonia vapor stream (mass fraction 99.8%), and the poor solution at the bottom of the GEN enters the SHR2 to heat the basic solution and is subsequently depressurized before entering the ABS1; meanwhile, the ammonia vapor from the top of the RET condenses in the condenser (CON); then, the saturated liquid ammonia flows into the subcooler (SUC) to heat the ammonia vapor leaving the SUC, is throttled, and afterwards enters the evaporator (EVA) to produce refrigeration effect; the ammonia vapor leaving the SUC joins with the pressurized basic solution stream 17 and is remixed into a rich solution, and therefore, the whole system completed.

To simplify the analysis, some reasonable assumptions are made in this paper:

(1) The steady-state operating conditions are assumed, and the possible leakage and pressure drops in the connection pipes are neglected [24, 32]

(2) Heat dissipation to the surroundings in the main devices and pipes is neglected [24, 31]

(3) The stream states at the CON, ABS1, and ABS2 exit are assumed to be saturated, and the cooling water enters each device above at ambient temperature and pressure [24]

(4) Specific isentropic efficiencies are assumed in the pumps and turbines [32]

(5) The chilled water entering the EVA is assumed to be water under environmental conditions

3. Exergy and Exergoeconomic Analysis Model and Performance Evaluation Criteria of the System

3.1. Exergy Analysis Model and Performance Evaluation Criterion of the Novel System. The proposed system consists of various functional devices, turbines, compressors, and heat exchangers, for instance. And each component of the proposed system can be considered to be a controllable volume with inlet and outlet streams, energy transfer, and work interactions. Mass and exergy balance expressions based on the principle of the first and second law of each component at corresponding state points are provided for exergy analysis.

The total exergy rate of input heat and inlet exergy streams equals the total exergy rate of output work, outlet exergy streams, and irreversible exergy loss rate. Therefore, the exergy balance equation of an open, steady component with multiple inflow and outflow streams is summarized as follows [24]:

$$\dot{E}_{w,i} = \dot{E}_{q,i} + \sum \dot{E}_{\text{in},i} - \sum \dot{E}_{\text{out},i} - \dot{E}_{d,i}, \quad (1)$$

where $\dot{E}_{w,i}$ is the exergy rate associated with output work, $\dot{E}_{q,i}$ is the exergy rate associated with input thermal energy, $\dot{E}_{\text{in},i}$ and $\dot{E}_{\text{out},i}$ are the exergy rates associated with inlet and outlet flows, respectively, and $\dot{E}_{d,i}$ is the relevant exergy destruction rate.

For the inflow and outflow streams of each component, ignore the impact of magnetic, nuclear, electrical, and surface effects and neglect the changes in mechanical energy;

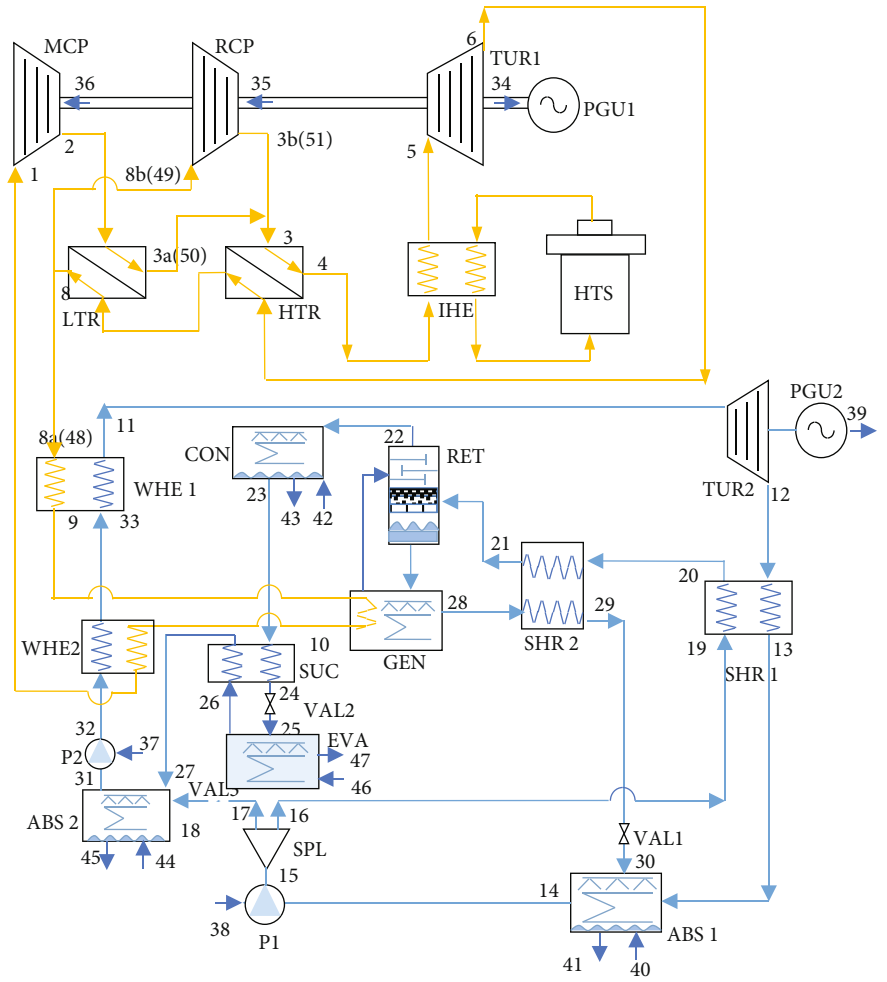

Figure 1: Schematic diagram of the completely recuperative SCO_2 Brayton absorption combined power/cooling cycle.

the exergy value of a certain stream is the sum of physical and chemical exergies. And exergy rate expression is as follows:

$$\dot{E} = \dot{E}_{ph} + \dot{E}_{ch}. \tag{2}$$

And the physical exergy can be expressed as [26]

$$\dot{E}_{ph} = \dot{m}[(h - h_{ref}) - T_{ref}(s - s_{ref})], \tag{3}$$

where the subscript ref stands for the reference state (surroundings) of CO_2 at 298.15 K and 0.1 MPa. And the chemical exergy of the ammonia-water mixture at different concentrations can be expressed as [26]

$$\dot{E}_{ch} = \dot{m}\left[\left(\frac{X}{M_{NH_3}}\right)e^0_{ch,NH_3} + \left(\frac{1-X}{M_{H_2O}}\right)e^0_{ch,H_2O}\right], \tag{4}$$

where X is the molar fraction of ammonia in the ammonia-water mixture and the M_{NH_3} and M_{H_2O} are the molar mass of ammonia and water, respectively. e^0_{ch,NH_3} and e^0_{ch,H_2O} are the standard reference chemical exergy values of ammonia and water, respectively [33].

To evaluate the proposed system from the first law perspective, the overall thermal efficiency of the combined system η_{en} can be expressed as [34]

$$\eta_{en} = \frac{\dot{W}_{net,brayton} + \dot{W}_{net,absorption} + \dot{Q}_{refrigeration}}{\dot{Q}_{input}}, \tag{5}$$

where $\dot{W}_{net,brayton}$, $\dot{W}_{net,absorption}$, and $\dot{Q}_{refrigeration}$ are, respectively, the net power output for the Brayton subcycle, the net power output for the absorption power/cooling subcycle, and the cooling capacity associated with the refrigeration output in EVA. $\dot{Q}_{input}$ is the supplied heat associated with the heat source in HTS.

To evaluate the proposed system from the second law perspective, the exergy efficiency of the combined system η_{ex} can be defined as [34]

$$\eta_{ex} = \frac{\dot{W}_{net,brayton} + \dot{W}_{net,absorption} + \dot{E}_{refrigeration}}{\dot{E}_{input}}, \tag{6}$$

where $\dot{E}_{\text{refrigeration}}$ is the exergy associated with the refrigeration effect. $\dot{E}_{\text{input}}$ is the exergy associated with the heat source in HTS. These are expressed as

$$\dot{E}_{\text{refrigeration}} = \dot{E}_{25} - \dot{E}_{26} = \dot{m}_{25}[(h_{25} - h_{26}) - T_{\text{ref}}(s_{25} - s_{26})],$$
$$\dot{E}_{\text{input}} = \dot{Q}_{\text{input}}\left(1 - \frac{T_{\text{ref}}}{T_{\text{HTS}}}\right). \tag{7}$$

Instead of the conventional temperate effectiveness definition based on the constant isobaric specific heat capacity assumption in classical heat exchanger design guides, the physical property variation of SCO_2 in HTR and LTR is too dramatic to ignore; therefore, the definition of enthalpy effectiveness is adopted and expressed as [35]

$$\varepsilon_{\text{HTR}} = \frac{\dot{m}_6(h_6 - h_7)}{\dot{m}_6(h_6 - h_{7\,\min}(P_7, T_3))} = \frac{\dot{m}_3(h_4 - h_3)}{\dot{m}_6(h_6 - h_{7\,\min}(P_7, T_3))},$$
$$\varepsilon_{\text{LTR}} = \frac{\dot{m}_7(h_7 - h_8)}{\dot{m}_6(h_6 - h_{7\,\min}(P_7, T_3))} = \frac{\dot{m}_2(h_3 - h_2)}{\dot{m}_6(h_6 - h_{7\,\min}(P_7, T_3))}. \tag{8}$$

3.2. Exergoeconomic Analysis Model and Performance Evaluation Criterion of the Novel System. For the reason that energy analysis and economic analysis are incapable of revealing the irreversibility and economic feasibility of the combined system under investigation, an exergoeconomic analysis that provides in-depth insights into the unit exergetic cost of each product stream is conducted. And the principle of exergoeconomic balance equations, as well as essential auxiliary equations of each functional component, is provided. The overall cost rate of input heat exergy, inlet exergy streams, and equipment expenditure is equal to the total cost rate of output work and outlet exergy streams. For system equipment that absorbs heat and generates electricity, the cost rate of the exergoeconomic balance equation can be recorded as [36]

$$\sum \dot{C}_{\text{out},i} + \dot{C}_{w,i} = \sum \dot{C}_{\text{in},i} + \dot{C}_{q,i} + \dot{Z}_i, \tag{9}$$

where $\dot{C}_{\text{out},i}$ and $\dot{C}_{\text{in},i}$ are the terms related to the output and input exergetic cost rates of each stream, respectively. $\dot{C}_{w,i}$ is the exergetic cost rate of output work, $\dot{C}_{q,i}$ is the exergetic cost rate of input heat, and $\dot{Z}_i$ is the cost rate of equipment expenditure.

$$\dot{C} = c * \dot{E}, \tag{10}$$

where c is the specific exergetic cost rate of each stream.

$$\dot{Z}_i = \dot{Z}_i^{\text{CI}} + \dot{Z}_i^{\text{OM}}, \tag{11}$$

where $\dot{Z}_i^{\text{CI}}$ and $\dot{Z}_i^{\text{OM}}$ are the cost rate terms related to annualized capital investment and operation and maintenance, respectively. For $\dot{Z}_i^{\text{CL}}$,

$$\dot{Z}_i^{\text{CL}} = \left(\frac{\text{CRF}}{\tau}\right) Z_{\text{i}}, \tag{12}$$

where CRF is the capital recovery factor and τ is the annual system operation time 8000 h [36]. And the relevant expressions are expressed as follows:

$$\text{CRF} = \frac{i_r(1 + i_r)^n}{(1 + i_r)^n - 1}. \tag{13}$$

And i_r is the annualized interest rate (10%) and n is the system effective operational period (20 years).

$$Z_i^{\text{OM}} = \gamma_i Z_i + \omega_i E_{p,i} + R_i, \tag{14}$$

where γ_i and ω_i are the fixed and alterable operation and maintenance expenditure and R_i is the unanticipated operation and maintenance costs in addition to equipment investment and product exergy. In the last two terms in equation (14) which are profoundly smaller ones, they are frequently neglected in published works of literature, and the same strategy is adopted in the present work; consequently, the γ_i is fixed at 0.06 [37].

To evaluate the proposed system from the exergy economics point of view, the specific cost of the product exergy streams for the whole system $c_{\text{P,total}}$ is expressed as

$$c_{\text{P,total}} = \frac{\sum_{i=1}^{n_f} c_{\text{fi}} \dot{E}_{\text{fi}} + \sum_{i=1}^{n_k} \dot{Z}_k}{\sum_{i=1}^{n_p} \dot{E}_{\text{pi}}}, \tag{15}$$

where n_f, n_k, and n_p are the entire terms related to the fuel exergy streams, system components, and product exergy streams for the whole system, respectively.

The detailed exergoeconomic balance equations and relevant auxiliary equations for each component in the proposed system are expressed in Table 6 in the appendix, and the relevant calculation models of Z_i are provided in Table 7 in the appendix. The components downstream of the throttle values and expansion value are regarded as an integrated component for that the relevant definition of throttling products is unclear. And the costs of the valves and SPL are ignored due to the relatively smaller proportion of total investment. It is worth pointing out that the heat exchangers most commonly adopted for the Brayton subcycle are printed circuit heat exchangers (PCHE) [10, 38]. Compared to typical bulky shell and tube exchangers, PCHE are novel compact microchannel plate exchangers which are assumed to have excellent pressure and temperature resistance but relatively much higher prices. To calculate the required equipment investment accurately, a material of SUS316L and the cost price of 50 \$/kg of the bonded block core are assumed, and the typical sizes for etched channel diameter, channel spacing, and plate thickness of 1.5 mm,

0.5 mm, and 1.5 mm are adopted in the cost calculation, and the detailed schematic model of the cross section and geometry dimension feature of the PCHE is illustrated in Figure 14 in the appendix. Moreover, the definition of integral mean temperature difference (IMTD) and calculation of heat transfer area is illustrated in Figure 15 in the appendix.

Assume the specific exergetic cost of the entering cooling water stream of CON, ABS1, ABS2, and EVA to be 0 $/GJ [39]. Therefore, exergetic cost equations of relevant fuel and product exergy streams can be obtained, and the linear systems of equations listed in Table 6 in the appendix consist of 51 variables $\{\dot{C}_1, \dot{C}_2, \dot{C}_3, \dot{C}_{3a}, \dot{C}_{3b}, \dot{C}_4, \ldots, \dot{C}_8, \dot{C}_{8a}, \dot{C}_{8b}, \ldots, \dot{C}_{47}\}$ and 51 equations and are solved using the open-source library package Scipy 1.7 under Python environment.

On the basis of the above mathematical analysis model, a simulation procedure is built and implemented on the Python 3.7 platform, and the fluid properties are calculated using the open-source library package CoolProp.

3.3. Model Validation. For model validation purposes, since there hardly exists a thermal system with consistent layout and parameter operation ranges in published pieces of literature, the SCO_2 Brayton subcycle and the absorption power/cooling subcycle within the proposed system are verified individually. And the detailed comparison results are listed in Tables 1 and 2.

To validate the established model built for the proposed system, the performance results of the SCO_2 recompression Brayton subcycle are compared with the available published literature data by Cheng et al. [40]. And the satisfying agreement is reached for the comparison results illustrated in Table 1.

For the absorption power/cooling subcycle, a published literature data by Zheng et al. [41] with the similar operation and functional characteristic is built, as the mass flow rate information for each state point is not provided and the mass flow rate of the working medium at the turbine inlet is set as 1 kg/s for the sake of contrastive analysis. As can be seen from Table 2, the thermal and exergy efficiency of the reference system is 24.24% and 37.28%, respectively; the corresponding energy and exergy efficiency of the built procedure is 24.0% and 38.7%, respectively. The main reasons for the deviations are the differences brought by the thermal physical property programs and rounding error.

In general, the comparison results in Tables 1 and 2 agree well with those reported in published literature; therefore, the accuracy of the built procedure is valid.

4. Results and Discussion

4.1. Parametric Sensitivity Analysis. A parametric sensitivity analysis is carried out for the proposed combined power/cooling cycle to reveal the impacts on thermal efficiency, exergy efficiency, and the specific cost of the product exergy streams for the whole system. The key parameters concerned include TUR1 inlet temperature, TUR1 inlet pressure, WHE1 outlet degree of overheat, WHE1 pitch point difference, TUR2 inlet pressure, TUR2 inlet ammonia concentration, GEN outlet temperature, and ABS1 outlet ammonia concentration. And the basic initial input parameters for the base case system performance evaluation are summarized in Table 3.

Table 1: Cycle parameter assumptions and efficiency value comparison for the Brayton system.

Cycle parameters	Values
MCP inlet temperature (K)	305.15
MCP inlet pressure (MPa)	7.38
TUR1 inlet temperature (K)	823.15
TUR1 inlet pressure (MPa)	25
Compressor isentropic efficiency	0.89
Turbine isentropic efficiency	0.93
Heat exchanger effectiveness	0.95
Pressure ratio	3.4
Cycle efficiency in Cheng et al.'s study [40]	39.82%
Cycle efficiency in the present study	39.78%

The mass flow rate of the SCO_2 Brayton subcycle m_5 is assumed to be 2500 kg/s, and the molar fraction of ammonia vapor at the top exit of the RET x_{22} is 0.998, which can be treated as pure ammonia. And the detailed information for the thermodynamic properties of each state point is summarized in Table 8 in the appendix.

The effects of TUR1 inlet temperature T_5 on thermal efficiency, exergy efficiency, and the specific cost of the product exergy streams for the proposed system (represented by solid symbols) and typically SCO_2 recompression Brayton cycle (represented by hollow symbols) are depicted in Figure 2. With the increase in the T_5, for the Brayton power module, the generated electricity of the TUR1 is on the increase, the outflow enthalpy of the HTR is on the increase, and the enthalpy values of H_8, H_{3a}, and H_2 remain constant, due to that split ratio = $1 - (h_7 - h_8)/(h_{3a} - h_2)$; the split ratio is on the decrease; therefore, the power consumption of the MCP is on the increase, while that of the RCP is on the decrease, and the total consumption of the two compressors is on the decrease; the thermal efficiency, the exergy efficiency, and the net output capacity are on the increase. Moreover, compared to the increase rate of the cost of fuel exergy streams and the system components, the exergetic cost rate of the products increases significantly at relatively low heat source temperatures; therefore, the specific cost of product exergy streams declines sharply, and further benefits of increasing T_5 are negligible for inlet temperature above 800 K. For the thermal efficiency, the net power output, the refrigeration output, and the supplied heat increase with T_5, the relative increase in overall output capacity is greater than the thermal energy supply; the maximum thermal efficiency can reach up to 71.35% at the T_5 of 923.15 K. For the exergy efficiency, take the inlet temperatures of 646, 670, and 692 K for example, the overall exergy output is 67.00, 82.66, and 98.12 MW, the thermal exergy input is 162.67, 178.57, and 194.70 MW, and the relative increase in input exergy is 15.67, 15.90, and 16.13 MW, while the relative increase in output exergy is 15.92, 15.67, and 15.46 MW, respectively; therefore, the promotion effect of inlet temperature on

Table 2: Cycle parameter and efficiency value comparison for two absorption systems.

Cycle parameters	Reference [41]		This article	
	Energy	Exergy	Energy	Exergy
Input heat Q_{bol} (kW)	3730	1946	2719.5	1185.8
Input heat Q_{gen} (kW)	667.3	204.5	338.9	118
Turbine generated work W_{tur} (kW)	774.7	774.7	474.8	474.8
Refrigeration capacity Q_{eva} (kW)	298.8	39.42	259.5	30.5
Pump input work P_1 (kW)	23.14	23.14	16.21	16.21
Pump input work P_2 (kW)	9.275	9.275	0	0
Pump input work P_3 (kW)	0	0	4.32	4.32
Overall efficiency (%)	24.24	37.28	24.0	38.7

Table 3: Main assumptions and initial input parameters for the base case system performance.

Parameters	Values
Ambient temperature (K)	298.15
Ambient pressure (kPa)	100
TUR2 inlet ammonia vapor concentration	0.79
TUR1 inlet temperature (K)	823.15
TUR1 inlet pressure (kPa)	25000
MCP inlet temperature (K)	308.15
MCP inlet pressure (kPa)	7400
GEN inlet temperature (K)	403.15
Minimum allowable dryness in the turbine exhaust	0.9
Compressor isentropic efficiency	0.85
Pump isentropic efficiency	0.87
Turbine isentropic efficiency	0.85
Refrigeration temperature (K)	280.15
Pinch point temperature difference (K)	10-20
Concentration of the basic solution (%)	0.42
TUR2 inlet degree of superheat (K)	5
Reactor fuel cost ($/MWh)	7.4

exergy efficiency is not so obvious under higher TUR1 inlet temperature; the maximum thermal efficiency can reach up to 67.31% at the T_5 of 923.15 K. For the specific cost of system products, although the cost of fuel exergy streams, system components, and the product exergy streams rise with T_5, the increase rate for the former two items is much smaller compared to that for the last item; hence, the variation for unit cost of system products is in a downward trend.

Figure 3 shows the effects of TUR1 inlet pressure P_5 on thermal efficiency, exergy efficiency, and the specific cost of the product exergy streams for the proposed system (represented by solid symbols) and typically SCO_2 recompression Brayton cycle (represented by hollow symbols). As can be seen from Figure 3, compared to the recompression Brayton cycle, the thermal efficiency, the exergy efficiency, and the specific cost of the product exergy streams are enhanced significantly, and the influences of P_5 on system performance display a similar tendency to that of TUR1 inlet temperature T_5, and the reasons behind are almost the same with the variation of TUR1 inlet temperatures.

For the recompression Brayton cycle, with the inlet pressure P_5 rises, the split ratio decreases from 0.56 to 0.40, and the mass flow rate which flows to the WHE1 and WHE2 is on the increase; the generated power in the TUR1 increases from 156 MW to 300.9 MW, while the power consumption in the MCP and the RCP increases from 24.2 MW to 77.2 MW and 81.5 MW to 126.38 MW, respectively. And the benefits of increasing P_5 are negligible for inlet pressure above 26 MPa. The combined system exhibits optimal unit product cost performance of 11.58 $/GJ under the inlet pressure of 29 MPa, and the maximum thermal efficiency and exergy efficiency reach 69.20% and 65.00%, respectively.

The variation of thermal efficiency, exergy efficiency, and the specific cost of the product exergy streams with TUR2 inlet pressure P_{11} is shown in Figure 4. As the TUR2 inlet pressure P_{11} rises from 2.5 MPa to 4.0 MPa, the thermal efficiency is linearly proportional to the TUR2 inlet pressure, and the overall trend of exergy efficiency is increasing; however, the increase rate gradually decreases. The split ratio of the combined system has a significant influence on the system performance; for the thermal efficiency, the increase in the split ratio results in a decrease in power consumption for the MCP and a sharp increase in the power consumption for the RCP; therefore, the net power output of the Brayton subcycle and the refrigeration output capacity are on the decrease, the net power output of the absorption power/cooling subcycle is on the increase, the overall output energy and the input heat capacity are on the decrease, and the combined effect is a proportional increase; the maximum thermal efficiency reaches 69.09%. For the exergy efficiency, the decrease rate of overall output exergy exceeds the corresponding decrease rate of input exergy, and the maximum exergy efficiency reaches 63.23%.

For the specific cost of system products, within the TUR2 inlet pressure range investigated, both the fuel cost streams, the specific cost rate of system components, and the specific cost rate of product exergy streams are on the decrease, and firstly, the decrease rate of the product exergy streams is higher than that of the former two items; therefore, the combined effect is a proportional increase; afterwards, the decrease rate of the fuel cost streams and the system components is equal to that of product exergy stream

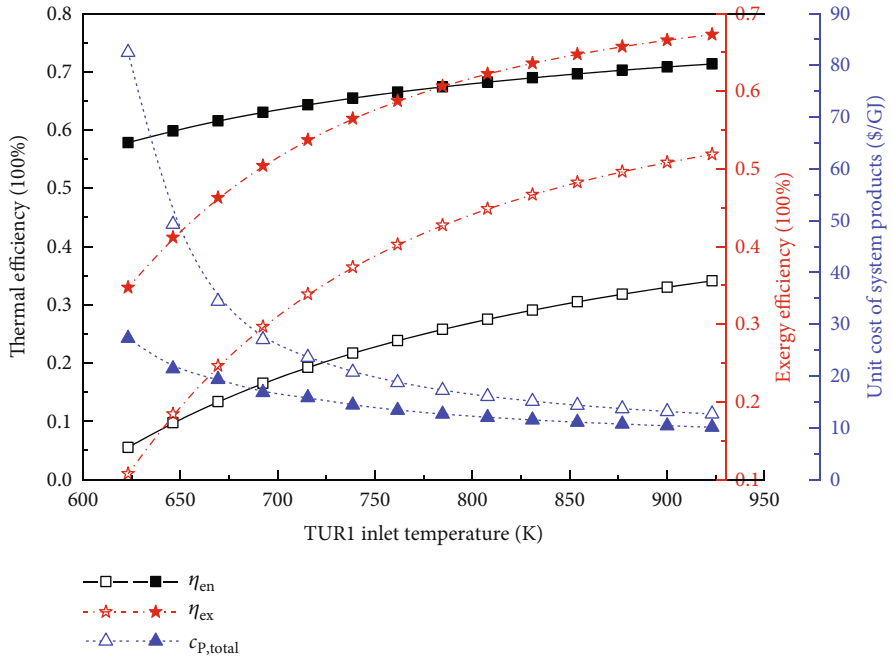

FIGURE 2: Variations of thermal efficiency, exergy efficiency, and specific cost of the product exergy streams with the system TUR1 inlet temperature T_5 for two systems.

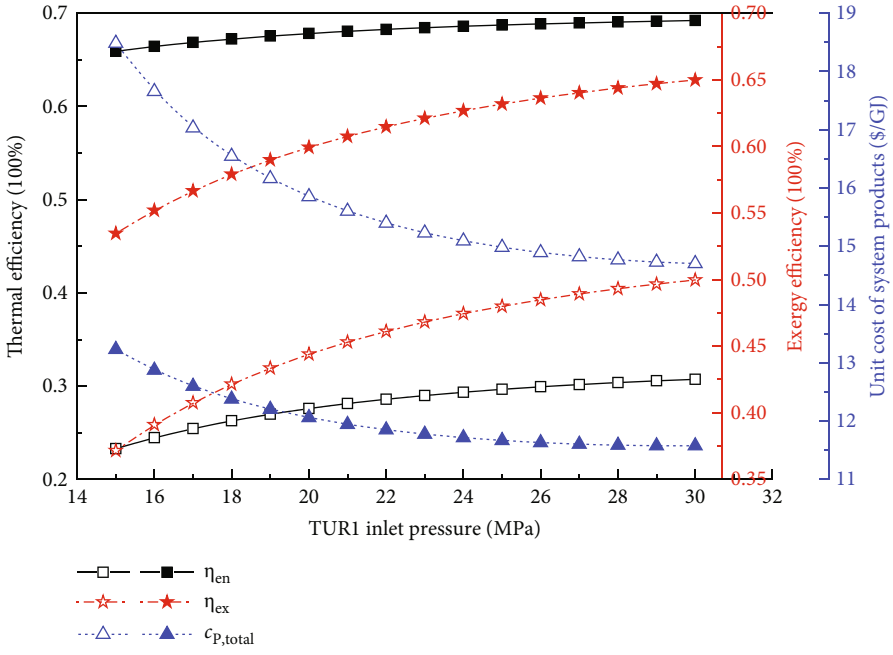

FIGURE 3: Variations of thermal efficiency, exergy efficiency, and specific cost of the product exergy streams with the system TUR1 inlet pressure P_5 for two systems.

cost at the TUR2 inlet pressure of 3.5 MPa, where the optimal unit product cost performance of 11.667 $/GJ is obtained.

The variation of thermal efficiency, exergy efficiency, and the specific cost of the product exergy streams with the degree of overheat ΔT_{11} and WHE1 pitch point difference ΔT_8 is illustrated in Figures 5 and 6. The variation curves of system performance for two temperature differences show an opposite tendency, and it is the coupling relationships between two subcycles that cause the appearance. To simplify the tedious analysis content, take the variation of thermal efficiency for WHE1 pitch point difference ΔT_8 for example. For the thermal efficiency, the split ratio is on the

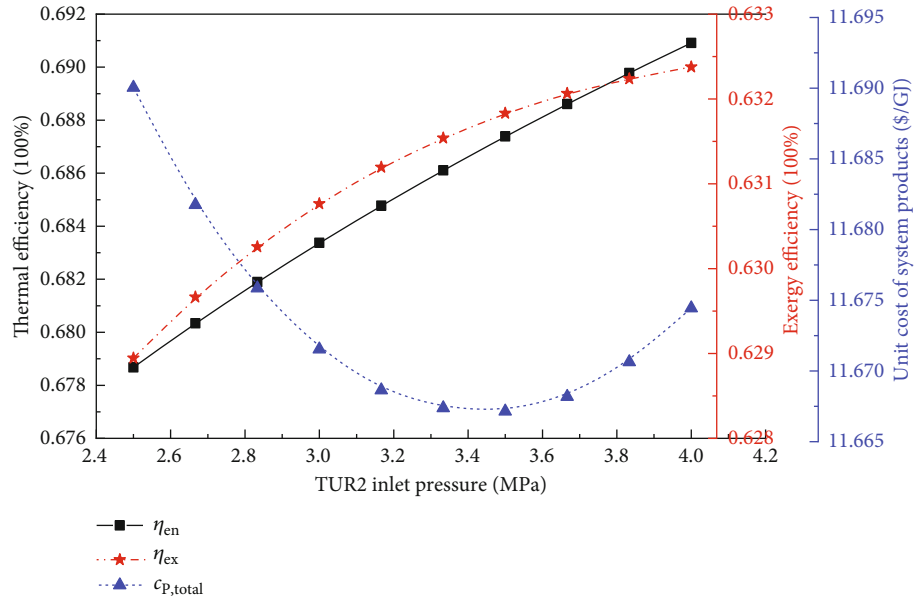

Figure 4: Variations of thermal efficiency, exergy efficiency, and specific cost of the product exergy streams with the system TUR2 inlet pressure P_{11}.

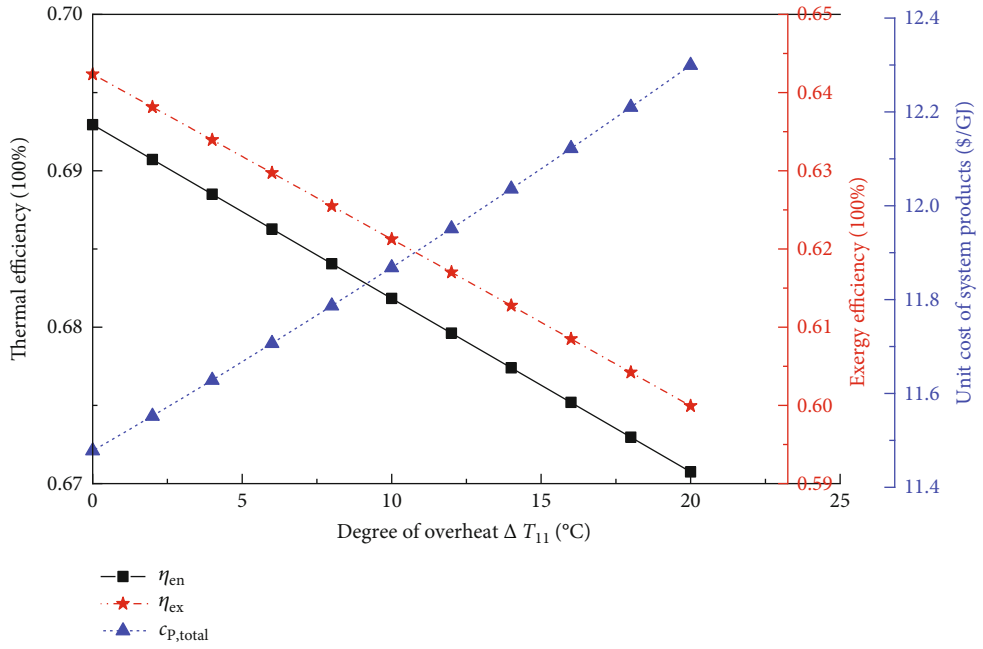

Figure 5: Variations of thermal efficiency, exergy efficiency, and specific cost of the product exergy streams with the system WHE1 outlet degree of overheat ΔT_{11}.

increase, the net power output of the Brayton subcycle is on the decrease, the mass flow rate of the absorption power/cooling subcycle rises from 189.3 to 191.2 kg/s, and the relevant energy output is on the increase; however, the input heat capacity decrease rate of 0.56% is lesser than that of 0.83% for the overall decrease rate of the proposed system; therefore, the thermal efficiency is inversely proportional to ΔT_8. For the specific cost of system products, the decrease rate of fuel cost streams and the system components drops from 0.57% to 0.40%, while the decrease rate of product exergy stream cost rises from 1.48% to 1.74%; the unit cost of system products rises from 11.52 to 13.63 $/GJ consequently. The maximum thermal efficiency and exergy efficiency reach 69.0% and 64.0%, respectively.

Figure 7 shows the variation of thermal efficiency, exergy efficiency, and the specific cost of the product exergy streams

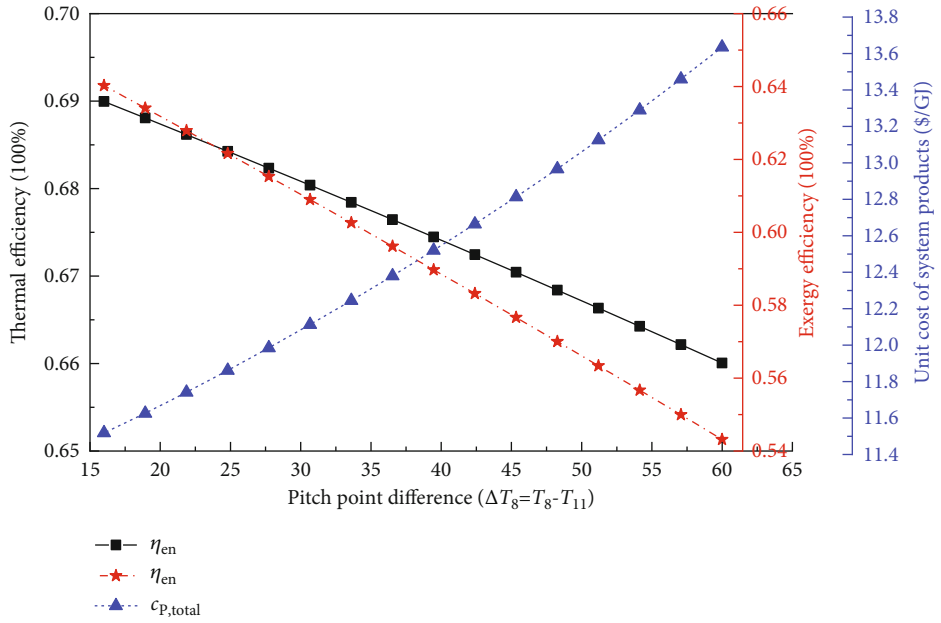

Figure 6: Variations of thermal efficiency, exergy efficiency, and specific cost of the product exergy streams with the system WHE1 pitch point difference ΔT_8.

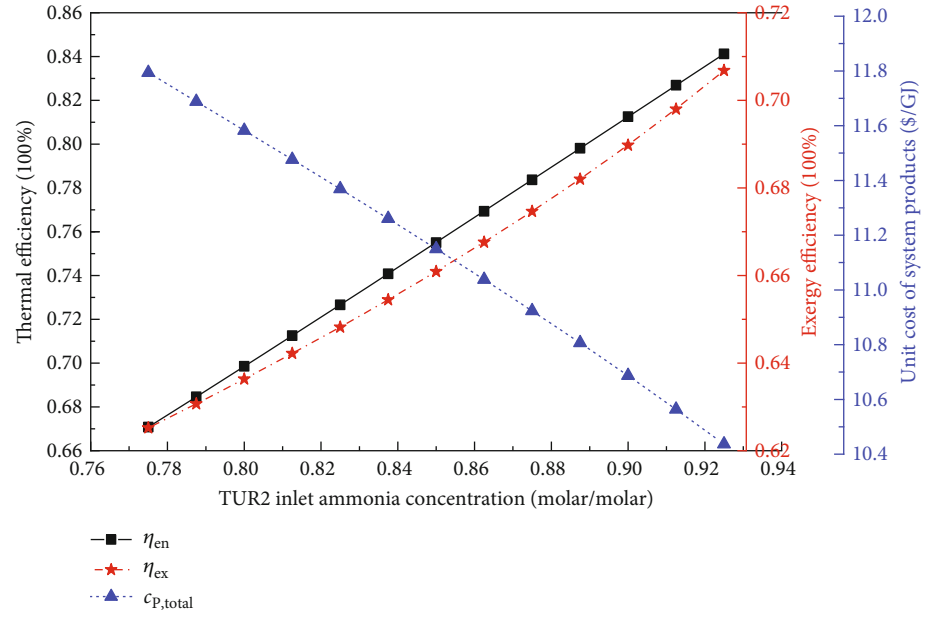

Figure 7: Variations of thermal efficiency, exergy efficiency, and specific cost of the product exergy streams with the system TUR2 inlet ammonia concentration X_{11} (molar fraction %).

with TUR2 inlet ammonia concentration X_{11}. As the X_{11} rises, the split ratio drops from 0.426 to 0.286, and the net power output of the Brayton subcycle increases from 136.4 to 175.5 MW, which has a dominant influence on the increase in overall energy output, and the increase rate is 4 times that of the supplied heat in the IHE; therefore, thermal efficiency and exergy efficiency increase from 67.1% to 84.1% and from 62.5% to 70.7%, respectively. For the specific cost of system products, the fuel cost streams and the system components rise from 4552.5 to 4882.1 \$/h and product exergy stream cost rises from 648.7 to 788.7 \$/h, but the minimum increase rate of the latter is 2 times larger than the former one; the unit cost of system products thereby decreases gradually.

Figure 8 presents the effects of GEN outlet temperature T_{10} on thermal efficiency, exergy efficiency, and the specific cost of the product exergy streams. As the GEN outlet temperature T_{10} rises, the net power output of the Brayton

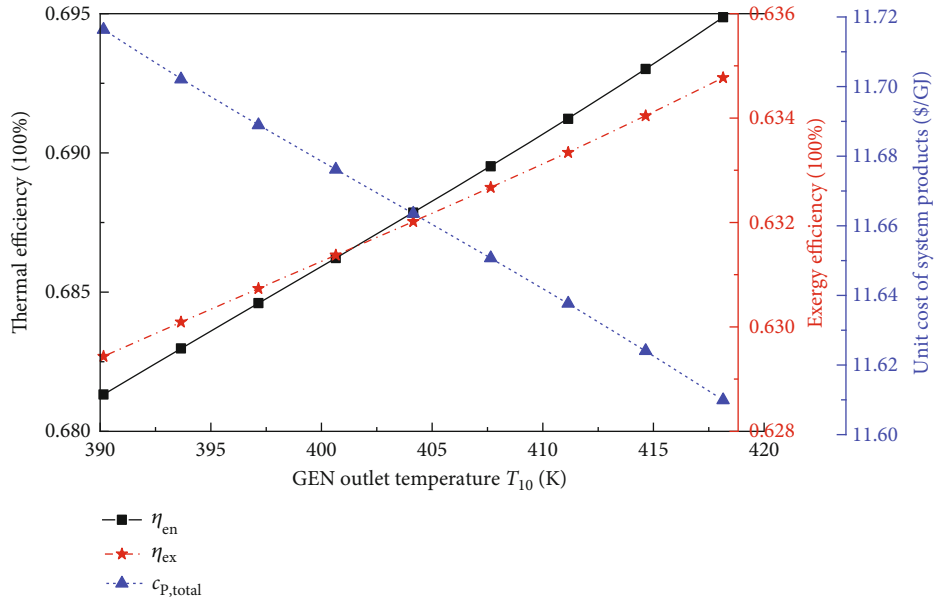

Figure 8: Variations of thermal efficiency, exergy efficiency, and specific cost of the product exergy streams with the system GEN outlet temperature T_{10}.

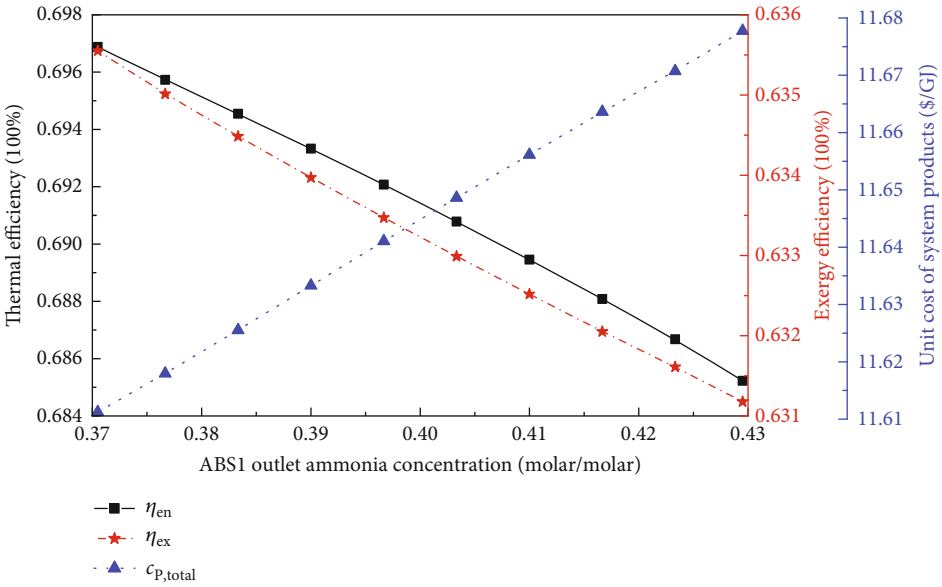

Figure 9: Variations of thermal efficiency, exergy efficiency, and specific cost of the product exergy streams with the system ABS1 outlet ammonia concentration X_{14} (molar fraction %).

subcycle, supplied heat, exergy, and exergy cost in the IHE remain unchanged, and energy output and exergy of the absorption power/cooling subcycle are on the increase; hence, the thermal efficiency and exergy efficiency are improving, and the maximum thermal efficiency and exergy efficiency reach 69.5% and 63.4%, respectively. For the specific cost of system products, the exergy cost of the system components is on the decrease and the product exergy streams cost is on the increase, and the unit cost of products drops consequently. And the minimum specific cost of system products reaches 11.61 $/GJ.

The variation of thermal efficiency, exergy efficiency, and the specific cost of the product exergy streams with ABS1 outlet ammonia concentration X_{14} is shown in Figure 9. As the ABS1 outlet ammonia concentration rises, the net power output of the Brayton subcycle, supplied heat, exergy, and exergy cost in the IHE remain unchanged, and energy output and exergy of the absorption power/cooling subcycle are on the decrease; hence, the thermal efficiency and exergy efficiency are declining. For the specific cost of system products, the exergy cost of the system components and the product exergy streams cost is on the decrease, and the

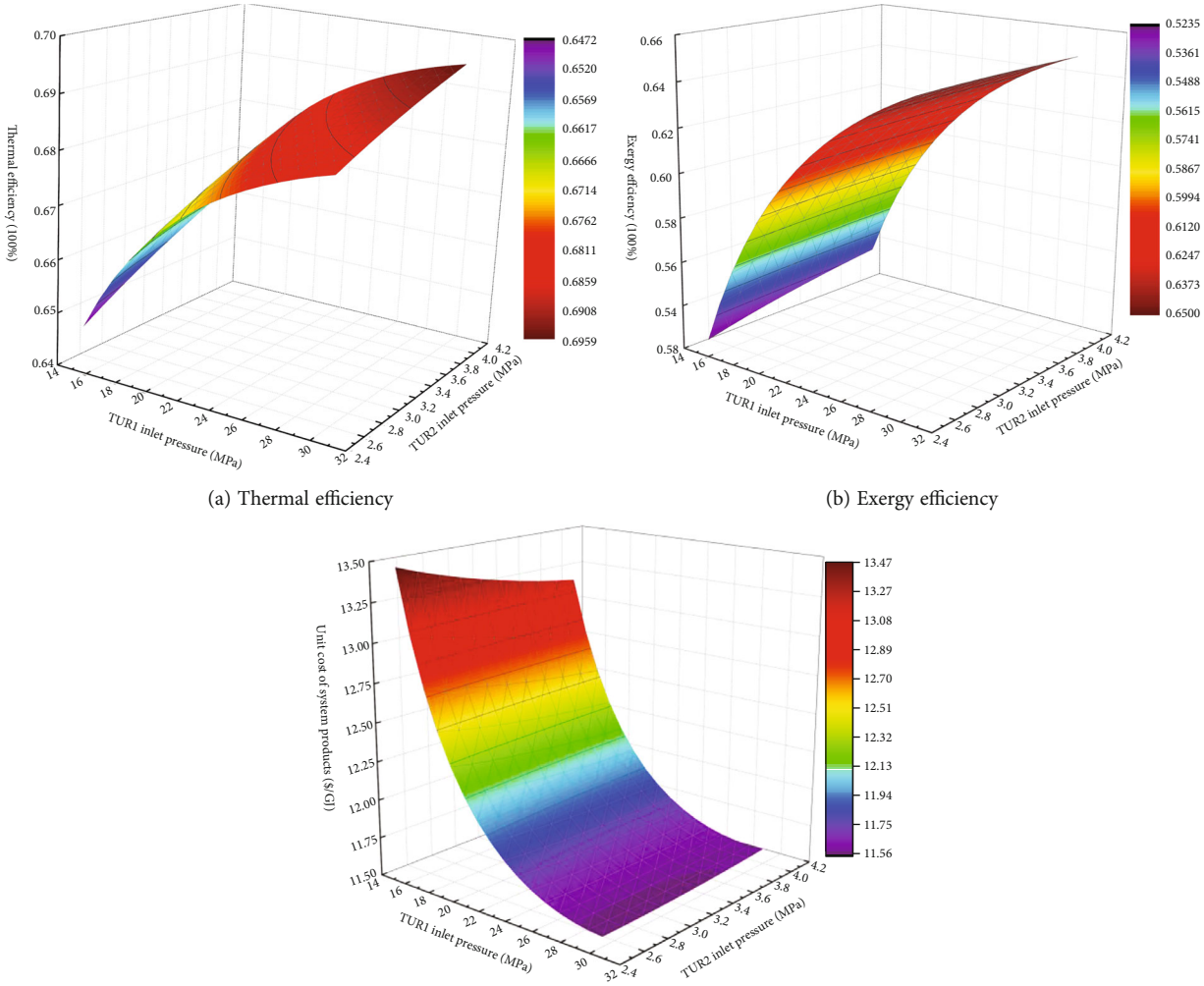

(a) Thermal efficiency

(b) Exergy efficiency

(c) The specific cost of the product exergy streams

Figure 10: Variations of system performance with the system TUR1 inlet pressure and TUR2 inlet pressure.

minimum increase rate of the latter is 1.8 times larger than the former one; hence, the unit cost of products declines consequently.

Since certain parameter variations have opposing effects on system performance, it is necessary to figure out the reasons behind them. Figure 10 presents the effects of TUR1 inlet pressure P_5 and TUR2 inlet pressure P_{11} on thermal efficiency, exergy efficiency, and the specific cost of the product exergy streams. The split ratio of the combined system rises with the TUR2 inlet pressure P_{11} and drops with the TUR1 inlet pressure P_5, and the related influence of TUR1 inlet pressure P_5 is weaker than that of TUR2 inlet pressure P_{11}. Figure 10(a) shows that the cycle will exhibit a maximum thermal performance of 69.5% under the specified condition when P_5 and P_{11} reach 30 and 4 MPa, respectively. For the exergy efficiency, TUR1 inlet pressure P_5 has a stronger influence on the exergy efficiency; therefore, the system can achieve higher overall exergy efficiency under lower P_5 and higher P_{11}, which favors the feasibility of implementation. For the specific cost of system products, as illustrated in Figures 3 and 4, TUR1 inlet pressure P_5 and TUR2 inlet pressure P_{11} have extremely inverse impacts on the unit cost of products, and it is apparent that there exists an optimal unit product cost under the TUR1 inlet pressure P_5 of 29 MPa, and the minimum unit product cost reaches 11.57 $/GJ.

The variation of thermal efficiency, exergy efficiency, and the specific cost of the product exergy streams with TUR1 inlet temperature T_5 and WHE1 pitch point difference ΔT_8 is depicted in Figure 11. For thermal efficiency, exergy efficiency, and the specific cost of system products, as illustrated in Figures 2 and 6, T_5 and ΔT_8 have extremely opposite impacts. The split ratio and mass flow rate of the absorption power/cooling subcycle are two factors influencing the coupling relationships and overall system performance, the split ratio of the combined system rises with the WHE1 pitch point difference ΔT_8 and drops with the TUR1 inlet temperature T_5, and the absorption power/cooling subcycle mass flow rate rises with T_5 and ΔT_8. However, the related influence of ΔT_8 is weaker than that of T_5. Figure 11(a) shows that the cycle exhibits a maximum thermal performance of 71.6% under the specified condition when T_5 and ΔT_8 reach 923.15 K and 16 K; moreover, the

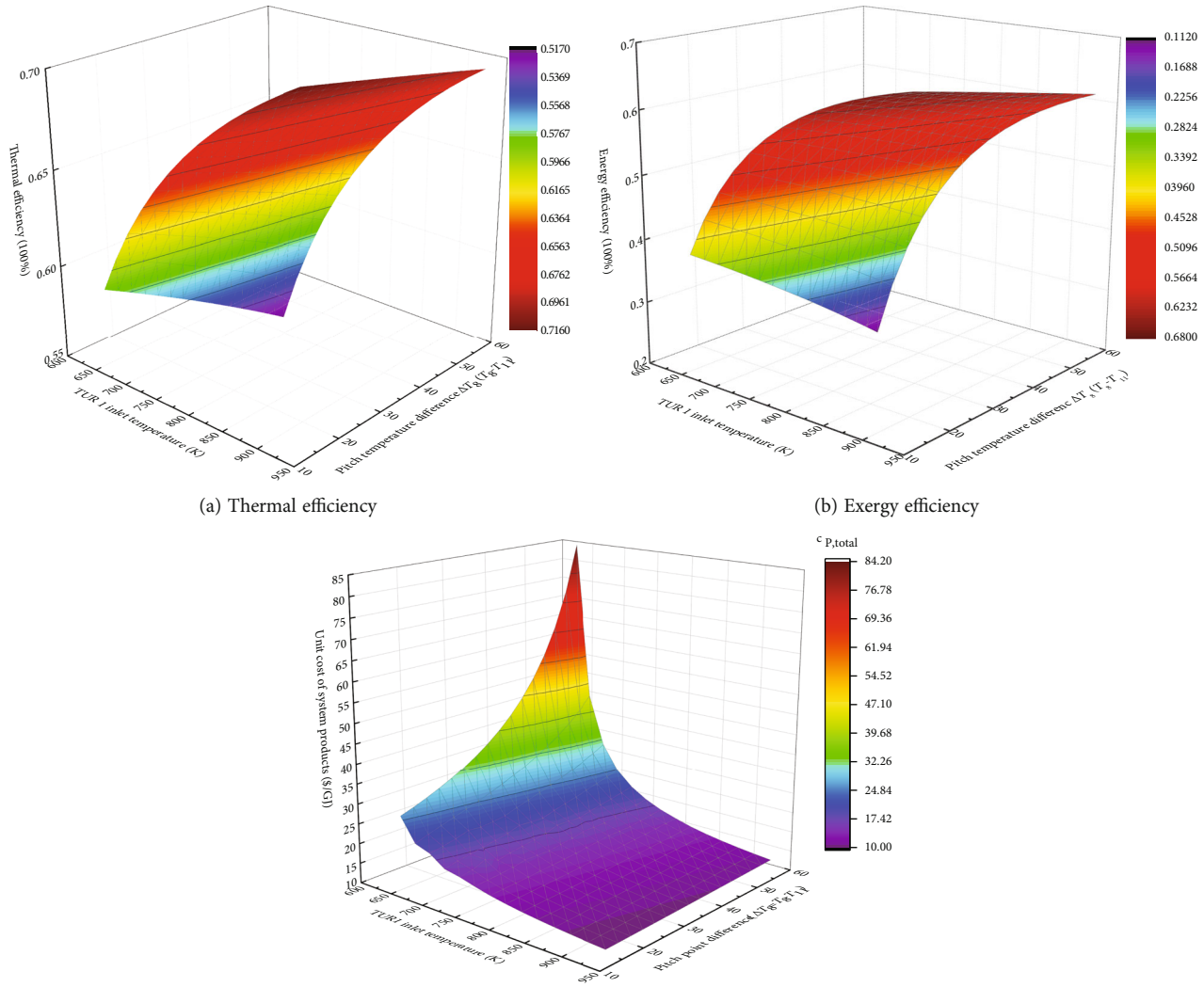

(a) Thermal efficiency

(b) Exergy efficiency

(c) Specific cost of the product exergy streams

FIGURE 11: Variations of system performance with the system TUR1 inlet temperature T_5 and WHE1 pitch point difference ΔT_8.

thermal efficiency and exergy efficiency gains under higher TUR1 inlet temperatures are extremely limited. For the specific cost of system products, it is evident that WHE1 pitch point difference ΔT_8 is the dominant affecting factor under lower T_5, and the minimum unit product cost reaches 10.02 \$/GJ.

The effects of TUR1 inlet temperature T_5 and GEN outlet temperature T_{10} on thermal efficiency, exergy efficiency, the specific cost of the product exergy streams and absorption power/cooling subcycle mass flow rate are illustrated in Figure 12. As shown in Figure 12(d), the mass flow rate of the absorption power/cooling subcycle rises with GEN outlet temperature T_{10} and the TUR1 inlet temperature T_5. For the thermal efficiency, however, the related influence of the GEN outlet temperature is weaker than that of the TUR1 inlet temperature. Figure 12(a) shows that the cycle exhibits a maximum thermal performance of 72% under the specified condition when T_5 and T_{10} reach 923.15 K and 418.15 K; moreover, GEN outlet temperature T_{10} has a negligible effect on the exergy efficiency, and relevant gains under higher TUR1 inlet temperatures are limited as well. For the specific cost of system products, it is evident that TUR1 inlet temperature T_5 is the dominant affecting factor, and the minimum unit product cost reaches 10.07 \$/GJ.

4.2. System Performance Optimization. For exergoeconomic evaluation of the combined system, the exergy destruction rate $\dot{E}_{d,i}$ and the cost rate of exergy destruction rate $\dot{C}_{d,i}$ are chosen as assessment criteria; these parameters are calculated for each component of the proposed system, and the detailed expression is expressed as follows:

$$\dot{C}_{d,i} = c_{f,i} * \dot{E}_{d,i}, \tag{16}$$

where $c_{f,i}$ is the unit cost of fuel exergy supplied for the specific component.

The objective function is to maximize η_{en} and η_{ex} or minimize $c_{P,total}$:

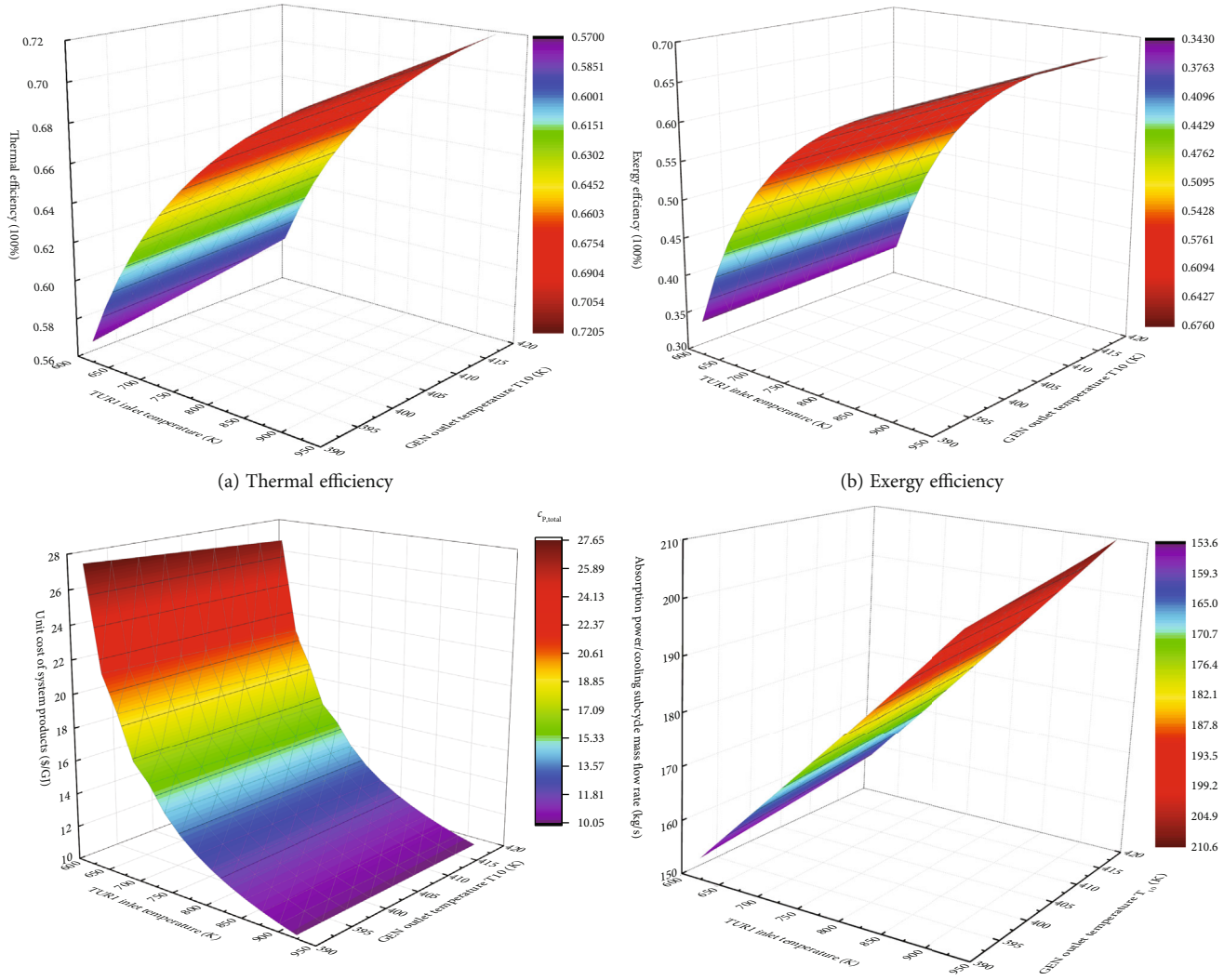

(a) Thermal efficiency

(b) Exergy efficiency

(c) The specific cost of the product exergy streams

(d) Absorption power/cooling subcycle mass flow rate

Figure 12: Variations of system performance with the TUR1 inlet temperature T_5 and GEN outlet temperature T_{10}.

$$
\begin{aligned}
623.15 \le T_5 \le 923.15,\\
15 \le P_5 \le 30,\\
2.5 \le P_{11} \le 4,\\
0 \le \Delta T_{11} \le 20,\\
15 \le \Delta T_8 \le 60,\\
0.775 \le X_{11} \le 0.925,\\
383.15 \le T_{10} \le 418.15,\\
0.37 \le X_{14} \le 0.43.
\end{aligned}
\tag{17}
$$

And the optimal parameter selection of the decision variables and system performance for the thermal efficiency case, the exergy efficiency case, the unit cost of product case, and the base case are illustrated in Table 4. Compared to the base case, three optimal cases exhibit remarkably improvement in thermal efficiency, exergy efficiency, and refrigeration capacity, and the exergy efficiency case is a promising candidate for moderate maximum operating temperature and pressure. Moreover, relevant thermal efficiency, exergy efficiency, and the unit cost of products of the exergy efficiency case are 82.44%, 72.35%, and 5.805 $/GJ, respectively, which are 13.7% and 9.17% higher for the first two items and 83.66% lower for the last item than that of the base case.

Figure 13 presents the contribution proportion of each component in the relevant cost rate $\dot{Z}_i$, the exergy destruction rate $\dot{E}_{d,i}$, and the cost rate of exergy destruction $\dot{C}_{d,i}$ for the base case, η_{en} case, η_{ex} case, and $c_{P,total}$ case, respectively. TUR1 and MCP account for the first- and second-largest cost rate for each case, RET and GEN make up roughly 34% exergy destruction rate and 20% cost rate of exergy destruction rate in three optimal cases, and reducing heat transfer difference in relevant equipment can further promote the system performance.

Table 4: Optimal parameter selection of the decision variables for different objective cases.

Parameters	Base case	Optimal cases		
		η_{en} case	η_{ex} case	$c_{p,total}$ case
TUR1 inlet temperature T_5 (K)	823.15	827.33	867.85	920.41
TUR1 inlet pressure P_5 (MPa)	25	26.51	25.56	28.20
TUR2 inlet pressure P_{11} (MPa)	3.5	3.95	2.97	2.84
WHE1 outlet degree of overheat ΔT_{11} (K)	5	2.23	2.1	5.46
WHE1 pitch point difference ΔT_8 (K)	20	46.45	15.36	20.76
TUR2 inlet ammonia concentration X_{11}	0.79	0.924	0.917	0.901
GEN outlet temperature T_{10} (K)	130	137.4	115.6	116.85
ABS1 outlet ammonia concentration X_{14}	0.42	0.41	0.43	0.38
Split ratio $m_{8b}/(m_{8a}+m_{8b})$	0.418	0.375	0.205	0.216
Brayton subcycle output work (MW)	139.05	156.88	215.10	249.34
Absorption subcycle output work (MW)	40.79	43.36	35.80	39.16
Absorption subcycle refrigeration capacity (MW)	142.42	218.89	210.02	215.17
Absorption subcycle mass flow rate (kg/s)	189.47	211.62	206.91	215.65
Thermal efficiency η_{en}	68.74%	84.79%	82.44%	81.41%
Exergy efficiency η_{ex}	63.18%	67.16%	72.35%	72.16%
Unit cost of the system products $c_{p,total}$ ($/GJ)	11.667	11.016	9.489	9.456

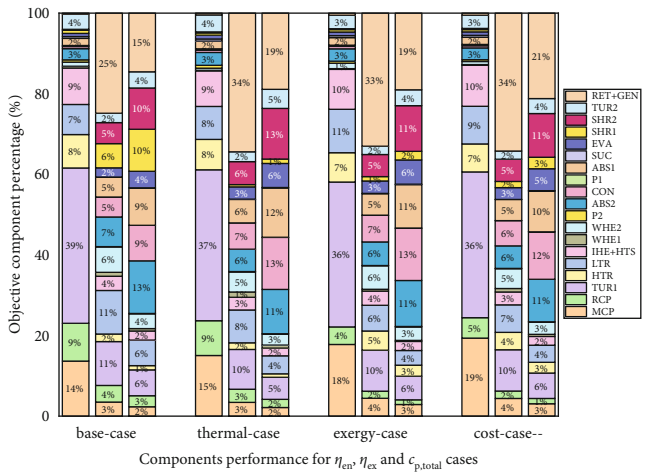

Figure 13: Exergoeconomic evaluation on each component of the combined system for different objective cases.

For multiobjective optimal parameter selection purposes, considering that contradictory goals exist in the optimization process and the ambiguous feature of the Pareto-GA method, a more straightforward approach to weighting each objective function is used [36]. And the integrated objective function is expressed as follows:

The objective function is to maximize $(w_1 \times \eta_{en} + w_2 \times \eta_{ex} + w_3 \times (1 - c_{p,total}/c_{reactor}))$:

$$0 \le w_1, w_2, w_3 \le 1,$$
$$w_1 + w_2 + w_3 = 1. \quad (18)$$

And the relevant weighting factors w_1, w_2, and w_3 on the synthetical performance of the multiobjective functions are listed in Table 5. Of the three multiobjective optimal cases, case 1 is based on the average weight of η_{en}, η_{ex}, and $c_{P,total}$, while the remaining cases add weights to the specific cost of system products; nevertheless, results show that the decision variable selection of the three multiobjective optimal cases is approaching, and the major deviations lie in the TUR1 inlet pressure P_5 and WHE1 pitch point difference ΔT_8. Therefore, the ultimate system scheme and optimal parameter values can be confirmed with flexibility in the optional deviation variables.

Table 5: Optimal values and objective functions of the decision variables and multiobjective functions.

Parameters	Multiobjective optimal cases		
	Case 1	Case 2	Case 3
w_1	1/3	0.1	0.4
w_2	1/3	0.4	0.1
w_3	1/3	0.5	0.5
TUR1 inlet temperature T_5 (K)	883.2	893.13	898.97
TUR1 inlet pressure P_5 (MPa)	28.94	26.44	26.28
TUR2 inlet pressure P_{11} (MPa)	3.2	3.4	4.0
WHE1 outlet degree of overheat ΔT_{11} (K)	2.62	4.37	6.70
WHE1 pitch point difference ΔT_8 (K)	23.56	28.43	20.17
TUR2 inlet ammonia concentration X_{11}	0.91	0.90	0.90
GEN outlet temperature T_{10} (K)	136.9	125.87	120.35
ABS1 outlet ammonia concentration X_{14}	0.38	0.39	0.39
Synthetical performance	60.2%	47.3%	51.6%
Thermal efficiency η_{en}	83.38%	82.36%	82.33%
Exergy efficiency η_{ex}	71.6%	70.8%	71.8%
Unit cost of the system products $c_{p,total}$ (\$/GJ)	9.663	9.866	9.686

5. Conclusions

In this paper, a completely recuperative SCO_2 Brayton/absorption integrated power/cooling system is proposed in which the low-grade waste heat extracted from the PRC of the Brayton subcycle is completely recovered to generate additional electrical and cold energy. Based on the decision parameters, the performances of the integrated system are evaluated and optimized through the exergoeconomic approach. Furthermore, the main conclusions are summarized as follows:

(1) Thermal efficiency and exergy efficiency are positively related to TUR1 inlet temperature, pressure, TUR2 inlet pressure, TUR2 inlet ammonia concentration, and GEN outlet temperature. The unit cost of products is positively correlated with WHE1 outlet degree of overheat, WHE1 outlet degree of overheat, and ABS1 outlet ammonia concentration, and within the key parameter variation scopes investigated, there exists an optimal TUR2 inlet pressure of 3.5 MPa

(2) The TUR2 inlet temperature, the WHE1 outflow overheat degree, and the WHE1 hot end temperature difference have significant influences on the split ratio; however, unreasonable high effectiveness in relevant equipment has adverse effects on net output capacity decreases and the unit cost of products

(3) Compared to the base case, three optimal cases exhibit remarkable improvement in thermal efficiency, exergy efficiency, and refrigeration capacity. And the exergy efficiency case is a promising candidate for η_{en}, $\eta_{ex,}$ and $c_{P,total}$ of 82.44%, 72.35%, and 9.489 \$/GJ, respectively

(4) Exergy destruction and cost rate distribution of each component for three optimal cases reveal that TUR1 and MCP account for the first- and second-largest cost rate, while the RET and GEN make up roughly 34% of exergy destruction rate, and reducing heat transfer difference in relevant equipment can further promote the system performance

(5) In conclusion, integrating with the absorption power/cooling subcycle instead can significantly improve the system performance and environmental condition adaptability, especially at efficient utilization of low- and medium-temperature renewable energy sources. Therefore, the ultimate system scheme and optimal parameter values can be confirmed with flexibility in the optional deviation variables

Appendix

The detailed exergoeconomic balance equations and relevant auxiliary equations for each component in the proposed system are expressed in Table 6. The capital investment models are listed in Table 7 for each component of the proposed system [27]. The costs of throttling values VAL1 and VAL2 and splitter SPL are ignored for that the required expenditures are smaller compared to the remaining components, and the detailed information for the thermodynamics properties of each state point is summarized in Table 8.

For the capital cost of PCHE for HTR, LTR, and IHE, the required heat transfer area is calculated in an integral mean temperature difference method. Taking into account the impact of property variation, the relevant heat transfer areas are better evaluated by integral mean temperature difference (IMTD) instead of logarithmic mean temperature difference

Table 6: Exergoeconomic balance equations and auxiliary equations for the combined cycle.

Components	Exergoeconomic balance equations	Auxiliary equations
MCP	$\dot{C}_2 = \dot{C}_1 + \dot{C}_{36} + \dot{Z}_{\mathrm{MCP}}$	$\frac{\dot{C}_{34}}{\dot{E}_{34}} = \frac{\dot{C}_{36}}{\dot{E}_{36}}$
RCP	$\dot{C}_{3b} = \dot{C}_{8b} + \dot{C}_{35} + \dot{Z}_{\mathrm{RCP}}$	$\frac{\dot{C}_{34}}{\dot{E}_{34}} = \frac{\dot{C}_{35}}{\dot{E}_{35}}$
TUR1	$\dot{C}_6 + \dot{C}_{34} = \dot{C}_5 + \dot{Z}_{\mathrm{TUR1}}$	$\frac{\dot{C}_6}{\dot{E}_6} = \frac{\dot{C}_5}{\dot{E}_5}$
IHE+HTS	$\dot{C}_5 = \dot{C}_4 + \dot{Z}_{\mathrm{HTS}}$	/
HTR	$\dot{C}_4 + \dot{C}_7 = \dot{C}_6 + \dot{C}_3 + \dot{Z}_{\mathrm{HTR}}$	$\dot{C}_6/\dot{E}_6 = \dot{C}_7/\dot{E}_7;\ \dot{C}_3 = \dot{C}_{3a} + \dot{C}_{3b}$
LTR	$\dot{C}_8 + \dot{C}_{3a} = \dot{C}_7 + \dot{C}_2 + \dot{Z}_{\mathrm{LTR}}$	$\dot{C}_8/\dot{E}_8 = \dot{C}_7/\dot{E}_7;\ \dot{C}_8/\dot{E}_8 = \dot{C}_{8b}/\dot{E}_{8b} = \dot{C}_{8a}/\dot{E}_{8a}$
WHE1	$\dot{C}_{11} + \dot{C}_9 = \dot{C}_{8a} + \dot{C}_{33} + \dot{Z}_{\mathrm{WHE1}}$	$\frac{\dot{C}_{8a}}{\dot{E}_{8a}} = \frac{\dot{C}_9}{\dot{E}_9}$
WHE2	$\dot{C}_1 + \dot{C}_{33} = \dot{C}_{10} + \dot{C}_{32} + \dot{Z}_{\mathrm{WHE2}}$	$\frac{\dot{C}_{10}}{\dot{E}_{10}} = \frac{\dot{C}_1}{\dot{E}_1}$
P2	$\dot{C}_{32} + \dot{C}_{31} = \dot{C}_{37} + \dot{Z}_{\mathrm{P2}}$	$\frac{\dot{C}_{37}}{\dot{E}_{37}} = \frac{\dot{C}_{39}}{\dot{E}_{39}}$
ABS2+VAL3	$\dot{C}_{31} + \dot{C}_{45} = \dot{C}_{17} + \dot{C}_{27} + \dot{C}_{44} + \dot{Z}_{\mathrm{ABS2+VAL3}}$	$\frac{\dot{C}_{31}}{\dot{E}_{31}} = \frac{(\dot{C}_{27} + \dot{C}_{18})}{(\dot{E}_{27} + \dot{E}_{18})}$ $\dot{C}_{17}/\dot{E}_{17} = \dot{C}_{18}/\dot{E}_{18};\ \dot{C}_{44}/\dot{E}_{44} = 0$
P1	$\dot{C}_{15} = \dot{C}_{14} + \dot{C}_{38} + \dot{Z}_{\mathrm{P1}}$	$\frac{\dot{C}_{38}}{\dot{E}_{38}} = \frac{\dot{C}_{39}}{\dot{E}_{39}}$
ABS1+VAL1	$\dot{C}_{14} + \dot{C}_{41} = \dot{C}_1 + \dot{C}_{29} + \dot{C}_{40} + \dot{Z}_{\mathrm{ABS1+VAL1}}$	$\frac{\dot{C}_{14}}{\dot{E}_{14}} = \frac{(\dot{C}_{30} + \dot{C}_{13})}{(\dot{E}_{30} + \dot{E}_{13})}$ $\dot{C}_{29}/\dot{E}_{29} = \dot{C}_{30}/\dot{E}_{30};\ \dot{C}_{40}/\dot{E}_{40} = 0$
CON	$\dot{C}_{23} + \dot{C}_{43} = \dot{C}_{42} + \dot{C}_{22} + \dot{Z}_{\mathrm{CON}}$	$\dot{C}_{22}/\dot{E}_{22} = \dot{C}_{23}/\dot{E}_{23};\ \dot{C}_{42}/\dot{E}_{42} = 0$
SUC	$\dot{C}_{24} + \dot{C}_{27} = \dot{C}_{26} + \dot{C}_{23} + \dot{Z}_{\mathrm{SUC}}$	$\frac{\dot{C}_{26}}{\dot{E}_{26}} = \frac{\dot{C}_{27}}{\dot{E}_{27}}$
EVA+VAL2	$\dot{C}_{26} + \dot{C}_{47} = \dot{C}_{24} + \dot{C}_{46} + \dot{Z}_{\mathrm{EVA+VAL2}}$	$\frac{\dot{C}_{24}}{\dot{E}_{24}} = \frac{\dot{C}_{25}}{\dot{E}_{25}}$ $\dot{C}_{25}/\dot{E}_{25} = \dot{C}_{26}/\dot{E}_{26};\ \dot{C}_{46}/\dot{E}_{46} = 0$
SHR1	$\dot{C}_{20} + \dot{C}_{13} = \dot{C}_{12} + \dot{C}_{19} + \dot{Z}_{\mathrm{SHR1}}$	$\frac{\dot{C}_{12}}{\dot{E}_{12}} = \frac{\dot{C}_{13}}{\dot{E}_{13}}$
SHR2	$\dot{C}_{21} + \dot{C}_{29} = \dot{C}_{20} + \dot{C}_{28} + \dot{Z}_{\mathrm{SHR2}}$	$\frac{\dot{C}_{28}}{\dot{E}_{28}} = \frac{\dot{C}_{29}}{\dot{E}_{29}}$
TUR2	$\dot{C}_{12} + \dot{C}_{39} = \dot{C}_{11} + \dot{Z}_{\mathrm{TUR2}}$	$\frac{\dot{C}_{11}}{\dot{E}_{11}} = \frac{\dot{C}_{12}}{\dot{E}_{12}}$
RET+GEN	$\dot{C}_{22} + \dot{C}_{10} + \dot{C}_{28} = \dot{C}_{21} + \dot{C}_9 + \dot{Z}_{\mathrm{GEN+RET}}$	$\frac{(\dot{C}_{22} - \dot{C}_{21})}{(\dot{E}_{22} - \dot{E}_{21})} = \frac{(\dot{C}_{28} - \dot{C}_{21})}{(\dot{E}_{28} - \dot{E}_{21})}$ $\frac{\dot{C}_9}{\dot{E}_9} = \frac{\dot{C}_{10}}{\dot{E}_{10}}$
SPL	$\dot{C}_{15}/\dot{E}_{15} = \dot{C}_{16}/\dot{E}_{16};\ \dot{C}_{15}/\dot{E}_{15} = \dot{C}_{17}/\dot{E}_{17}$	$\frac{\dot{C}_{15}}{\dot{E}_{15}} = \frac{\dot{C}_{19}}{\dot{E}_{19}}$

Table 7: The capital investment models for each system component.

System component	The capital investment cost function
Reactor	$Z_r = c * \dot{Q}_r$, $c = 283$ \$/kWt
Turbine	$Z_t = 479.34 * \dot{m}_{in} * 1/0.93 - \eta_t * \ln(TR_t) * \left(1 + e^{0.036 * T_{in} - 54.4}\right)$
Compressor	$Z_c = 71.1 * \dot{m}_{in} * \frac{1}{0.92 - \eta_t} * PR_c * \ln(PR_c)$
Ammonia heat exchanger	$Z_h = 2143 * A_h^{0.514}$
Pump	$Z_p = 1120 * W_p^{0.8}$

Table 8: Thermodynamic properties, exergy streams, and unit cost of system products for the base case system performance.

State no.	T (K)	P (kPa)	$\dot{m}$ (kg/s)	x (%)	$\dot{E}$ (kW)	Cost rates	
						$\dot{C}$ (\$/h)	c (\$/GJ)
1	308.15	7400	1454.6	—	294,124.3	10,179.79	9.614
2	397.35	25300	1454.6	—	363,203.8	13,326.64	10.192
3	607.50	25200	2500.0	—	921,166.8	34,660.45	10.452
4	676.93	25100	2500.0	—	1030,651.3	38,704.54	10.432
5	823.15	25000	2500.0	—	1311,426.0	45,389.1	9.614
6	691.92	7750	2500.0	—	928,293.4	32,128.69	9.614
7	616.01	7650	2500.0	—	814,096.8	28,176.3	9.614
8	462.36	7550	2500.0	—	614,117.5	21,254.9	9.614
9	408.27	7500	1454.6	—	328,448.0	11,367.75	9.614
10	403.15	7450	1454.6	—	325,728.5	11,273.6	9.614
11	442.36	3500	184.31	0.790	3085,448.4	313,177.88	28.195
12	378.46	776.55	184.31	0.790	3037,536.5	308,314.80	28.195
13	315.25	776.55	184.31	0.790	3020,580.4	306,53.68	28.195
14	308.15	776.55	399.32	0.420	3498,188.8	361,000.3	28.666
15	308.23	1370.01	399.32	0.420	3498,483.4	361,042.32	28.666
16	308.23	1370.01	331.57	0.420	2904,905.6	299,785.3	28.666
17	308.23	1370.01	67.75	0.420	593,577.8	61,257.0	28.666
18	308.22	1366.76	67.75	0.420	580,184.2	59,874.82	28.666
19	308.23	1370.01	331.57	0.420	2904,905.6	299,785.28	28.666
20	328.31	1370.01	331.57	0.420	2906,771.8	301,515.0	28.813
21	365.63	1370.01	331.57	0.420	2929,718.1	302,641.96	28.695
22	328.66	1370.01	116.56	0.998	2406,557.9	249,698.3	28.822
23	308.15	1350.01	116.56	0.998	2394,094.6	248,405.11	28.822
24	296.05	1350.01	116.56	0.998	2394,003.8	248,410.73	28.823
25	280.15	553.63	116.56	0.998	2393,588.0	248,367.6	28.823
26	290.15	553.63	116.56	0.998	2384,604.7	247,435.46	28.823
27	305.56	553.63	116.56	0.998	2384,597.8	247,434.73	28.823
28	393.15	1370.01	215.01	0.090	463,297.1	53,040.69	31.801
29	334.79	1370.01	215.01	0.090	453,473.1	51,915.98	31.801
30	334.75	776.55	215.01	0.090	453.473.1	51,915.98	31.801
31	300.15	553.63	184.31	0.79	2999,946.2	310,954.44	28.793
32	300.79	3500.0	184.31	0.79	2992,549.6	311,069.0	28.874
33	400.33	3500	184.31	0.79	3040,074.4	312,173.68	28.524
$W_{brayton}$ (MW)		139.1	$W_{absorption}$ (MW)		40.8	$W_{refrigeration}$ (MW)	142.42
η_{en}		68.74%	η_{ex}		63.18%	$c_{P,total}$	11.67 \$/GJ

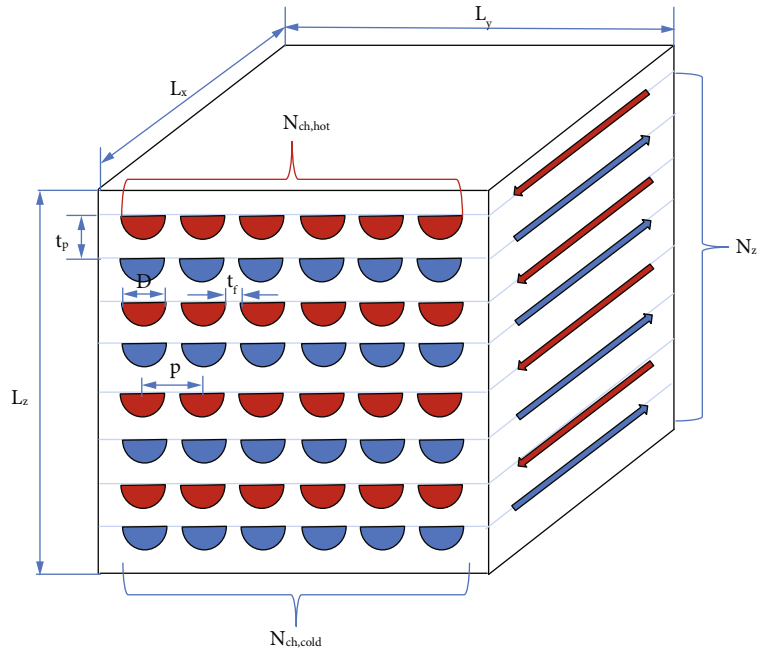

Figure 14: Schematic model of the cross section and geometry dimension feature of the PCHE.

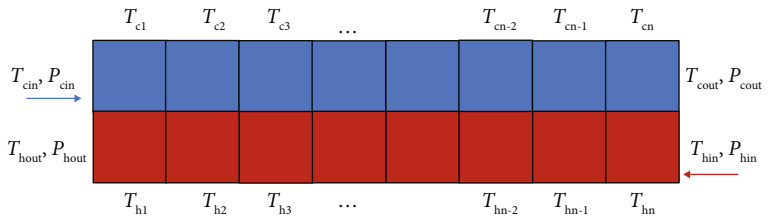

Figure 15: Nodalization subsection of heat exchanger.

(LMTD). As depicted in Figures 14 and 15, for modeling purposes, IMTD can be obtained by dividing the heat transfer length into infinitely small nodes to capture the effect of properties and integration of the local temperature difference.

$$dQ = U_i * dA_i * \Delta T,$$

$$\int_0^{Q_0} \frac{dQ}{\Delta T(Q)} = \int_0^{A_i} U_i * dA_i, \tag{A.1}$$

$$Q = U * A * TD_{\text{IMTD}},$$

Variables

c: Cost per exergy unit ($/GJ)
e: Specific exergy (kJ/kg)
h: Specific enthalpy (kJ/kg)
i_r: Annualized interest rate
$\dot{m}$: Mass flow rate (kg/s)
n: System effective operational period (year)
s: Specific entropy (kJ/(kg·K))
w: Weighting factor
$\dot{C}$: Exergy cost rate ($/h)
$\dot{E}$: Exergy rate (kW)
M: Molar mass (kg/mol)
P: Pressure (kPa)
$\dot{Q}$: Heat addition (kW)
R: Unanticipated operation and maintenance cost factor
T: Temperature (K)
$\dot{W}$: Work (kW)
X: Molar fraction of ammonia solution
$\dot{Z}$: Cost rate of equipment expenditure ($/h).

Greek Letters

γ: Fixed operation and maintenance expenditure
ΔT: Heat transfer temperature difference (K)
ε: Effectiveness
η: Thermal/exergy efficiency
τ: Annual system operation time
ω: Alterable operation and maintenance expenditure.

Subscripts and Abbreviations

0: Surroundings
1,2,…51: State points
absorption: Absorption power/cooling subcycle
brayton: Brayton subcycle
ch: Chemical

d, i:	Exergy destruction rate of the ith component
en:	Energy
ex:	Exergy
f:	Fuel exergy streams
in, i:	Inlet exergy flow rate of the ith component
input:	Input heat
net:	Net output work
out, i:	Outlet exergy flow rate of the ith component
p:	Product exergy streams
ph:	Physical
q, i:	Input heat of the ith component
ref:	Reference state
refrigeration:	Cooling capacity
w, i:	Output work of the ith component
ABS1:	Absorber 1
ABS2:	Absorber 2
CI:	Capital investment
CRF:	Capital recovery factor
EVA:	Evaporator
GEN:	Generator
H_2O:	Water
HTS:	High-temperature source
IHE:	Intermediate heat exchanger
LTR:	Low-temperature recuperator
MCP:	Main compressor
NH_3:	Ammonia
OM:	Operation and maintenance
P1:	Pump 1
P2:	Pump 2
PCHE:	Printed circuit heat exchanger
PGU1:	Power generation unit 1
PGU2:	Power generation unit 2
PRC:	Precooler
P,total:	Specific cost of the product exergy streams
RCP:	Recompression compressor
SHR1:	Solution heat recuperator 1
SHR2:	Solution heat recuperator 2
SPECO:	Specific exergy costing approach
SUC:	Subcooler
TEC:	Theory of the exergetic cost
TFA:	Thermoeconomic functional analysis
TUR1:	Turbine 1
TUR2:	Turbine 2
WHE1:	Waste heat recovery exchanger 1
WHE2:	Waste heat recovery exchanger 2.

Data Availability

The data used to support the finding of this study are included within the article. Further data or information is available via corresponding email from the corresponding/first author upon request.

Conflicts of Interest

The authors declare that they have no known competing financial interests or personal relationships that could have appeared to influence the work reported in this paper.

Authors' Contributions

Bingchuan Han wrote the original draft. Yongdong Chen was responsible for the conceptualization and supervision. Gaige Yu reviewed the paper. Xiaohong Wu was responsible for the validation. Qiushuang zhang was responsible for the software. Taotao Zhou was responsible for the model validation and syntax check.

Acknowledgments

We gratefully acknowledge the financial support for the grants of the Natural Science Foundation of Anhui Province (No. 2008085QE261), Key Research and Development Project of Anhui Province (No. 202104a05020024), and Doctoral Science and Technology Foundation of Hefei General Machinery Research Institute (No. 2020011748).

References

[1] J. Yang, Z. Yang, and Y. Duan, "Novel design optimization of concentrated solar power plant with S-CO_2 Brayton cycle based on annual off-design performance," *Applied Thermal Engineering*, vol. 192, article 116924, 2021.

[2] J. Yang, Z. Yang, and Y. Duan, "Part-load performance analysis and comparison of supercritical CO_2 Brayton cycles," *Energy Convers. Manage.*, vol. 214, article 112832, 2020.

[3] A. Yu, W. Su, X. Lin, and N. Zhou, "Recent trends of supercritical CO2 Brayton cycle: bibliometric analysis and research review," *Nuclear Engineering and Technology*, vol. 53, no. 3, pp. 699–714, 2021.

[4] D. Zhao, S. Deng, R. Zhao, L. Zhao, W. Xu, and X. Long, "The flexible programming of thermodynamic cycles: application of supercritical carbon dioxide Brayton cycles," *Energy Convers. Manage*, vol. 245, 2021.

[5] P. Wu, Y. Ma, C. Gao et al., "A review of research and development of supercritical carbon dioxide Brayton cycle technology in nuclear engineering applications," *Nuclear Engineering and Design*, vol. 368, p. 110767, 2020.

[6] H. Liu, Z. Chi, and S. Zang, "Transient behaviour and optimal start-up procedure of closed Brayton cycle with high thermal inertia," *Applied Thermal Engineering*, vol. 199, p. 117587, 2021.

[7] J. Yang, Z. Yang, and Y. Duan, "Load matching and techno-economic analysis of CSP plant with S-CO_2 Brayton cycle in CSP-PV-wind hybrid system," *Energy*, vol. 223, article 120016, 2021.

[8] K. Wang, M.-J. Li, Z.-D. Zhang, C.-H. Min, and P. Li, "Evaluation of alternative eutectic salt as heat transfer fluid for solar power tower coupling a supercritical CO2 Brayton cycle from the viewpoint of system-level analysis," *Journal of Cleaner Production*, vol. 279, article 123472, 2021.

[9] T. Xin, C. Xu, and Y. Yang, "Thermodynamic analysis of a novel supercritical carbon dioxide Brayton cycle based on the thermal cycle splitting analytical method," *Energy Conversion and Management*, vol. 225, article 113458, 2020.

[10] E. Ruiz-Casanova, C. Rubio-Maya, J. J. Pacheco-Ibarra, V. M. Ambriz-Díaz, C. E. Romero, and X. Wang, "Thermodynamic analysis and optimization of supercritical carbon dioxide Brayton cycles for use with low-grade geothermal heat sources,"

Energy Conversion and Management, vol. 216, article 112978, 2020.

[11] L. Zhang, T. Deng, J. J. Klemeš, M. Zeng, T. Ma, and Q. Wang, "Supercritical CO2 Brayton cycle at different heat source temperatures and its analysis under leakage and disturbance conditions," *Energy*, vol. 237, article 121610, 2021.

[12] S. I. Schöffer, S. A. Klein, P. V. Aravind, and R. Pecnik, "A solid oxide fuel cell- supercritical carbon dioxide Brayton cycle hybrid system," *Applied Energy*, vol. 283, article 115748, 2021.

[13] E. G. Feher, "The supercritical thermodynamic power cycle," *Energy Conversion*, vol. 8, no. 2, pp. 85–90, 1968.

[14] G. Angelino, "Carbon dioxide condensation cycles for power production," *Journal of Engineering for Gas Turbines Power*, vol. 90, pp. 85–90, 1968.

[15] B. Liu, M. Lu, B. Shui, Y. Sun, and W. Wei, "Thermal-hydraulic performance analysis of printed circuit heat exchanger precooler in the Brayton cycle for supercritical CO_2 waste heat recovery," *Applied Energy*, vol. 305, article 117923, 2022.

[16] H. Hu, Y. Jiang, C. Guo, and S. Liang, "Thermodynamic and exergy analysis of a S-CO2 Brayton cycle with various of cooling modes," *Energy Conversion and Management*, vol. 220, article 113110, 2020.

[17] Y. Cao, H. Habibi, M. Zoghi, and A. Raise, "Waste heat recovery of a combined regenerative gas turbine - recompression supercritical CO2 Brayton cycle driven by a hybrid solar-biomass heat source for multi-generation purpose: 4E analysis and parametric study," *Energy*, vol. 236, article 121432, 2021.

[18] J. Lian, D. Xu, H. Chang et al., "Thermal and mechanical performance of a hybrid printed circuit heat exchanger used for supercritical carbon dioxide Brayton cycle," *Energy Conversion and Management*, vol. 245, p. 114573, 2021.

[19] K. Cheng, J. Zhou, X. Huai, and J. Guo, "Experimental exergy analysis of a printed circuit heat exchanger for supercritical carbon dioxide Brayton cycles," *Applied Thermal Engineering*, vol. 192, article 116882, 2021.

[20] S. Khatoon, S. Ishaque, and M.-H. Kim, "Modeling and analysis of air-cooled heat exchanger integrated with supercritical carbon dioxide recompression Brayton cycle," *Energy Conversion and Management*, vol. 232, article 113895, 2021.

[21] Y. Liang, J. Chen, X. Luo, J. Chen, Z. Yang, and Y. Chen, "Simultaneous optimization of combined supercritical CO2 Brayton cycle and organic Rankine cycle integrated with concentrated solar power system," *Journal of Cleaner Production*, vol. 266, article 121927, 2020.

[22] K. A. Abrosimov, A. Baccioli, and A. Bischi, "Techno-economic analysis of combined inverted Brayton-organic Rankine cycle for high-temperature waste heat recovery," *Energy Conversion and Management*, vol. 207, article 112336, 2020.

[23] A. I. Kalina, "Combined cycle and waste heat recovery power systems based on a novel thermodynamic energy cycle utilizing low-temperature heat for power generation," in *1983 Joint Power Generation Conference: GT Papers*, p. 5, Indianapolis, Indiana, USA, 1983.

[24] J. Tang, Q. Zhang, Z. Zhang, Q. Li, C. Wu, and X. Wang, "Development and performance assessment of a novel combined power system integrating a supercritical carbon dioxide Brayton cycle with an absorption heat transformer," *Energy Conversion and Management*, vol. 251, article 114992, 2022.

[25] B. C. Han, W. L. Cheng, and Y. H. Huang, "Thermodynamic analysis of a novel ammonia-water power/cooling combined system with adjustable refrigeration-to-power ratio," *Energy Procedia*, vol. 158, pp. 2462–2468, 2019.

[26] A. Pirmohamadi, H. Ghaebi, B. M. Ziapour, and M. Ebadollahi, "Exergoeconomic analysis of a novel hybrid system by integrating the Kalina and heat pump cycles with a nitrogen closed Brayton system," *Energy Reports*, vol. 7, pp. 546–564, 2021.

[27] A. D. Akbari and S. M. S. Mahmoudi, "Thermoeconomic analysis & optimization of the combined supercritical CO_2 (carbon dioxide) recompression Brayton/organic Rankine cycle," *Energy*, vol. 78, pp. 501–512, 2014.

[28] R. P. Merchán, M. J. Santos, J. García-Ferrero, A. Medina, and A. C. Hernández, "Thermo-economic and sensitivity analysis of a central tower hybrid Brayton solar power plant," *Applied Thermal Engineering*, vol. 186, article 116454, 2021.

[29] D. Luo and D. Huang, "Thermodynamic and exergoeconomic investigation of various SCO_2 Brayton cycles for next generation nuclear reactors," *Energy Conversion and Management*, vol. 209, article 112649, 2020.

[30] Y. Zhao, M. Liu, J. Song, C. Wang, J. Yan, and C. N. Markides, "Advanced exergy analysis of a Joule-Brayton pumped thermal electricity storage system with liquid-phase storage," *Energy Conversion and Management*, vol. 231, article 113867, 2021.

[31] T. Zhou, Z. Liu, X. Li, M. Zhao, and Y. Zhao, "Thermodynamic design space data-mining and multi-objective optimization of SCO_2 Brayton cycles," *Energy Conversion and Management*, vol. 249, article 114844, 2021.

[32] A. Narasimhan, R. Kamal, and E. Almatrafi, "Novel synergetic integration of supercritical carbon dioxide Brayton cycle and adsorption desalination," *Energy*, vol. 238, p. 121844, 2022.

[33] I. Dincer and M. A. Rosen, *Exergy: Energy, Environment and Sustainable Development*, Newnes, 2nd edition, 2012.

[34] Y. Feng, Z. Du, M. Shreka, Y. Zhu, S. Zhou, and W. Zhang, "Thermodynamic analysis and performance optimization of the supercritical carbon dioxide Brayton cycle combined with the Kalina cycle for waste heat recovery from a marine low-speed diesel engine," *Energy Conversion and Management*, vol. 206, p. 112483, 2020.

[35] M. Saeed and M.-H. Kim, "A newly proposed supercritical carbon dioxide Brayton cycle configuration to enhance energy sources integration capability," *Energy*, vol. 239, article 121868, 2022.

[36] V. Zare, S. S. Mahmoudi, M. Yari, and M. J. E. Amidpour, "Thermoeconomic analysis and optimization of an ammonia-water power/cooling cogeneration cycle," *Energy*, vol. 47, no. 1, pp. 271–283, 2012.

[37] S. S. Mahmoudi, A. D. Akbari, and M. Rosen, "Thermoeconomic analysis and optimization of a new combined supercritical carbon dioxide recompression Brayton/Kalina cycle," *Sustainability*, vol. 8, no. 10, p. 1079, 2016.

[38] H. Xu, C. Duan, H. Ding et al., "The optimization for the straight-channel PCHE size for supercritical CO_2 Brayton cycle," *Nuclear Engineering and Technology*, vol. 53, no. 6, pp. 1786–1795, 2021.

[39] H. Li, M. Wang, J. Wang, and Y. Dai, "Exergoeconomic analysis and optimization of a supercritical CO2 cycle coupled with

a Kalina cycle," *Journal of Energy Engineering*, vol. 143, no. 2, article 04016055, 2017.

[40] W. Cheng, W. Huang, and Y. Nian, "Global parameter optimization and criterion formula of supercritical carbon dioxide Brayton cycle with recompression," *Energy Conversion and Management*, vol. 150, pp. 669–677, 2017.

[41] D. Zheng, B. Chen, Y. Qi, and H. Jin, "Thermodynamic analysis of a novel absorption power/cooling combined-cycle," *Applied Energy*, vol. 83, no. 4, pp. 311–323, 2006.